

# JGR Earth Surface

## RESEARCH ARTICLE

10.1029/2018JF004979

### Key Points:

- Cenozoic uplift history determined from calibrated inverse modeling of 4,161 North American river profiles
- Landscape modeling driven by this uplift history predicts drainage patterns, continental denudation, and sedimentary flux histories
- Incision estimates were tested using continent-wide inventory of thermochronometric measurements

### Supporting Information:

- Supporting Information S1

### Correspondence to:

V. M. Fernandes,  
v.fernandes17@imperial.ac.uk

### Citation:

Fernandes, V. M., Roberts, G. G., White, N., & Whittaker, A. C. (2019). Continental-scale landscape evolution: A history of North American topography. *Journal of Geophysical Research: Earth Surface*, 124, 2689–2722. <https://doi.org/10.1029/2018JF004979>

Received 20 DEC 2018

Accepted 3 SEP 2019

Accepted article online 6 SEP 2019

Published online 27 NOV 2019

## Continental-Scale Landscape Evolution: A History of North American Topography

Victoria M. Fernandes<sup>1</sup> , Gareth G. Roberts<sup>1</sup> , Nicky White<sup>2</sup>, and Alexander C. Whittaker<sup>1</sup>

<sup>1</sup>Department of Earth Science and Engineering, Imperial College London, London, UK, <sup>2</sup>Bullard Laboratories, Department of Earth Sciences, University of Cambridge, Cambridge, UK

The generation and evolution of continental topography are fundamental geologic and geomorphic concerns. In particular, the history of landscape development might contain useful information about the spatiotemporal evolution of deep Earth processes, such as mantle convection. A significant challenge is to generate observations and theoretical predictions of sufficient fidelity to enable landscape evolution to be constrained at scales of interest. Here, we combine substantial inventories of stratigraphic and geomorphic observations with inverse and forward modeling approaches to determine how the North American landscape evolved. First, stratigraphic markers are used to estimate postdepositional regional uplift. Present-day elevations of these deposits demonstrate that >2 km of long-wavelength surface uplift centered on the Colorado-Rocky-Mountain plateaus occurred in Cenozoic times. Second, to bridge the gaps between these measurements, an inverse modeling scheme is used to calculate the smoothest spatiotemporal pattern of rock uplift rate that yields the smallest misfit between 4,161 observed and calculated longitudinal river profiles. Our results suggest that Cenozoic regional uplift occurred in a series of stages, in agreement with independent stratigraphic observations. Finally, a landscape evolution model driven by this calculated rock uplift history is used to determine drainage patterns, denudation, and sedimentary flux from Late Cretaceous times until the present day. These patterns are broadly consistent with stratigraphic and thermochronologic observations. We conclude that a calibrated inverse modeling strategy can be used to reliably extract the temporal and spatial evolution of the North American landscape at geodynamically useful scales.

### 1. Introduction

Topography is the result of complex interactions between the solid Earth and surface processes that operate on multiple spatial and temporal scales (e.g., Anderson & Anderson, 2010; Roberts et al., 2019). Consequently, surface uplift and subsidence histories have been combined with magmatic and tomographic information to estimate temperatures, wavelengths, and timescales of mantle convection (e.g., Gurnis et al., 2000; Lodhia et al., 2018; Roberts et al., 2018; Salles et al., 2017; van Wijk et al., 2010). The results of these studies imply that mantle processes play a significant role in driving the erosional history of a landscape. Unfortunately, existing inventories of uplift or denudation measurements are sparse, which makes it difficult to determine histories of geodynamical processes (e.g., subplate support) at appropriate scales. Here, we explore how substantial biostratigraphic and thermochronologic compilations can be combined with stratigraphic information to constrain continental-scale surface uplift histories on time scales of  $O(1\text{--}100)$  Ma. We match insights from this approach with geomorphic observations to reconstruct a Cretaceous to Recent uplift history of the North American continent where subplate processes appear to have played an important role in generating and maintaining long-wavelength topography. Finally, we explore how calibrated rock uplift histories can be used to parameterize three-dimensional forward models of landscape evolution, which make predictions about continental denudation, drainage routing, and sedimentary flux that can be assessed using independent geologic observations.

Particular attention is paid to four regions with elevated topography: the Colorado-Columbia-Rocky Mountains plateaus, the Appalachian mountain belt, the Yukon plateau, and the Mexican highlands. Spot measurements of rock and surface uplift (e.g., uplifted marine stratigraphy, stable isotopes, paleoflora, and structural geology), denudation (e.g., low-temperature thermochronometry and fluvial incision dating), and the geochemistry of basaltic magmatism suggest that a broad region encompassing the Colorado-Rocky Mountain plateaus experienced multistaged Cenozoic uplift and denudation generated, at least in part, by

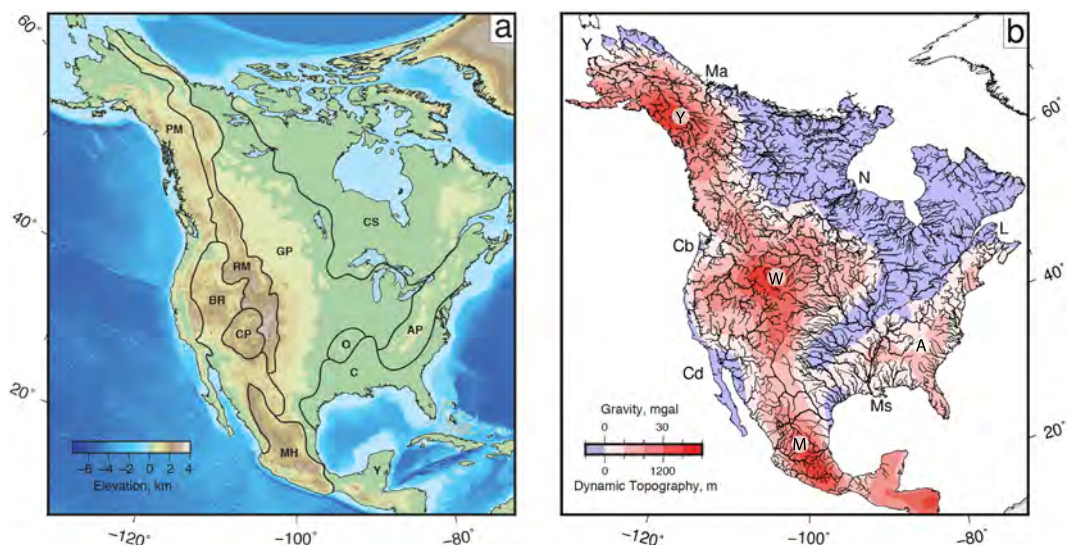


**Figure 1.** Topography, drainage, and dynamic support of North America. (a) Topographic map based upon ETOPO1 database where physiographic provinces are named using nomenclature of Fenneman (1928). PM = Pacific margin; RM = Rocky Mountains; BR = Basin and Range; CP = Colorado Plateau; GP = Great Plains; CS = Canadian Shield; O = Ozark-Ouachita Plateau; AP = Appalachian mountains; C = Gulf and Atlantic Coastal Plains; MH = Mexican Highlands. Albers Equal Area projection. (b) Thin black lines = 4161 rivers extracted from Advanced Space-borne Thermal Emission and Reflection Radiometer global digital elevation model database. Ms = mouth of Mississippi; L = St. Lawrence; N = Nelson; Ma = Mackenzie; Y = Yukon; Cb = Columbia; Cd = Colorado. Drainage network is draped over dynamic topography that is calculated from long-wavelength (i.e., <800 km) free-air gravity anomalies assuming admittance,  $Z=25$  mGal/km (GRACE mission database; Tapley et al., 2005, Stephenson et al., 2014). Labeled circles indicate centers of major swells. Y = Yukon; W = western North America; A = Appalachians; M = Mexico.

time-dependent thermal anomalies within the upper mantle (e.g., Chamberlain et al., 2012; Flowers et al., 2008; Huntington et al., 2010; Karlstrom et al., 2008; Mix et al., 2011; Sahagian, 1987). Punctuated delivery of clastic sediments into the Gulf of Mexico corroborate these observations (Galloway et al., 2011). There is also evidence for youthful regional uplift elsewhere. For example, uplifted Pliocene marine sedimentary rocks that crop out along the eastern seaboard and sedimentation rates within the Baltimore Canyon Trough imply that significant topography of the Appalachian mountains may have been generated during the last 20 million years (e.g., Poag & Sevon, 1989; Rowley et al., 2013). In the northern cratonic interior, thermochronometric observations and scattered outliers of Cretaceous marine sedimentary rock suggest several hundred meters of post-Cretaceous uplift and denudation occurred (e.g., Ault et al., 2013; Nassichuk & McIntyre, 1995). Widespread magmatism, uplifted marine terraces, and incised drainage patterns suggest that Mexico also experienced long-wavelength Cenozoic uplift (e.g., Stephenson et al., 2014). Nevertheless, the timing and mechanism for generating these patterns of regional uplift remain uncertain.

### 1.1. A Role for Large-Scale Crustal and Lithospheric Thickening?

Some models explain kilometer-scale changes in continental elevation by invoking crustal thickening by, for example, Early Cenozoic crustal flow (e.g., McQuarrie & Chase, 2000). These models have largely fallen out of favor since they are difficult to reconcile with present-day crustal thicknesses estimated from seismic wide-angle surveys, from receiver function analyses, and from shear wave dispersion modeling (e.g., Becker et al., 2014; Levander & Miller, 2012; Shen & Ritzwoller, 2016). Isostatic considerations would require the crust (and by inference the lithosphere) beneath the Colorado Plateau to be 1.7 times thicker than that beneath the Great Plains in order to generate the observed 1.5 km of relief (Figure 1a; Klocking et al., 2018; supporting information). However, empirical parametrization of shear wave tomographic models suggests that the lithospheric thickness beneath the Great Plains is approximately double that of the Colorado Plateau (e.g., Priestley & McKenzie, 2006; Shen & Ritzwoller, 2016). The striking similarity of crustal thicknesses beneath the Colorado-Columbia-Rocky Mountains plateaus and beneath the Great Plains (35–45 km) is consistent with the view that orogenesis played an insignificant role in

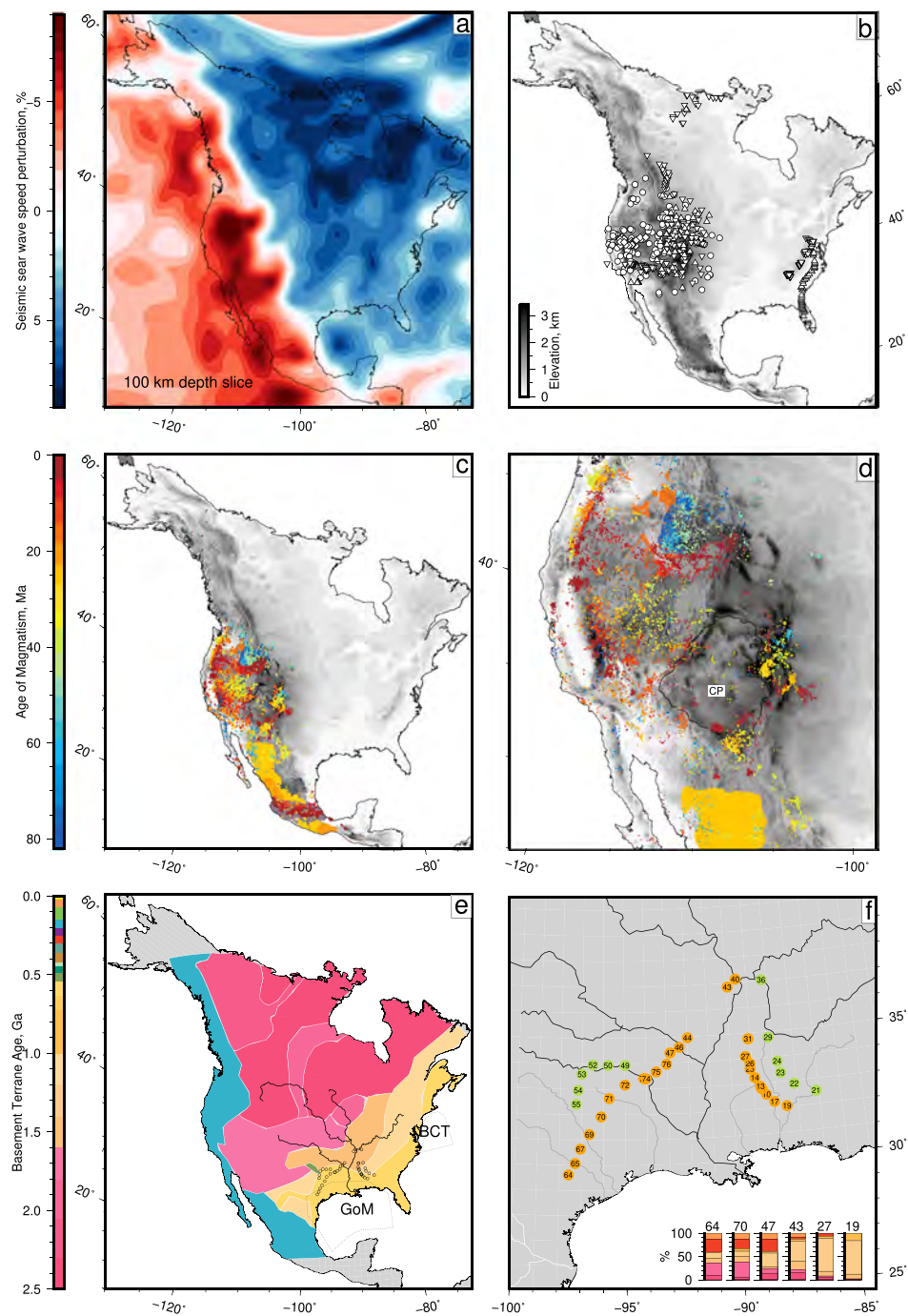


**Figure 2.** Mantle velocities, uplift, magmatism, and sedimentary provenance. (a) Shear wave speed anomalies beneath North America at depth of 100 km (Schaeffer & Lebedev, 2013). (b) Distribution of uplift (upward triangles), denudation (downward triangles), paleoaltimetry (circles), and paleoflow (squares) measurements since Late Cretaceous times (see text for references). (c) North American Cenozoic magmatism from NAVDAT database (Ferrari et al., 2012; [www.navdat.org](http://www.navdat.org)). Gray shading = present-day topography fromETOPO1 database; orange/yellow polygons = Oligocene/Miocene ignimbrites (Chapin et al., 2004; Ferrari et al., 1999). (d) Western North American magmatism centered on Colorado Plateau, which is outlined by black polygon labeled CP. (e) Basement terranes colored by age (after Blum & Pecha, 2014). Solid black lines = portion of present-day Mississippi drainage; circles = Cenomanian and Paleogene fluvial sandstones (Blum et al., 2017). Dotted polygons labeled GoM/BCT = Cenozoic clastic sedimentary deposition within Gulf of Mexico/Baltimore Canyon Trough (Galloway et al., 2011; Poag & Sevon, 1989). (f) Detrital zircons and drainage patterns along northern fringe of Gulf of Mexico. Black/gray/white lines = Mississippi/Texan/Mexican Rivers; labeled circles = subset of detrital zircon samples extracted from Cenomanian (green) or Paleocene-Eocene (orange) fluvial deposits. Inset with labeled bars = cumulative percentages of detrital zircon populations at locations that correspond to annotated circles on map. Colored circles = zircon ages (Blum et al., 2017).

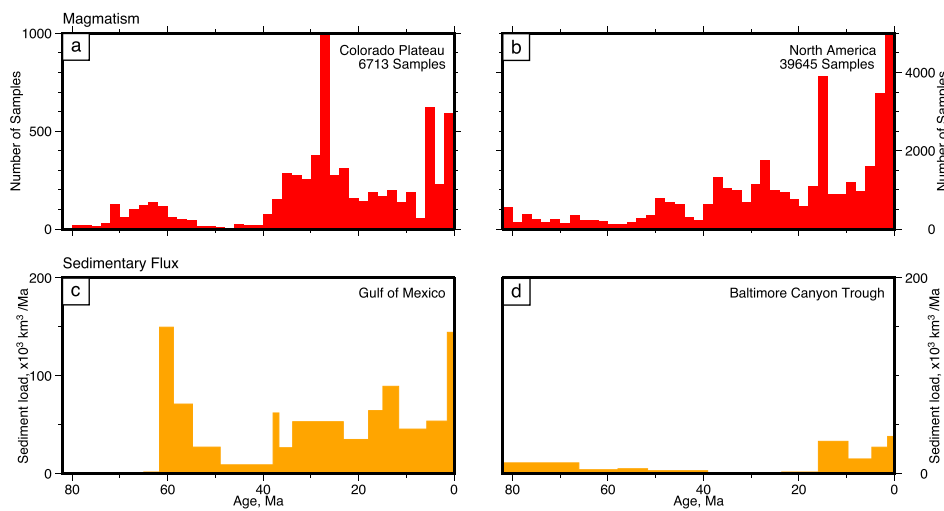


**Figure 3.** North American magmatism and sedimentary flux. (a) Magmatic record of Colorado Plateau taken from NAVDAT database. (b) Magmatic record of North America from NAVDAT database. (c) Solid sedimentary flux for Gulf of Mexico determined from seismic reflection surveys and well-log information by Galloway et al. (2011). (d) Uncorrected sedimentary flux for New Jersey margin determined from seismic reflection surveys and well-log information by Poag and Sevon (1989).

generating and maintaining the regional elevation of western North America since Late Cretaceous times (Spencer, 1996; Wilson et al., 2005). The observed velocity structure of the crust indicates that differences in crustal and sedimentary densities alone are insufficient to account for these dramatic changes in topographic relief (Klocking et al., 2018; Levandowski et al., 2018; Roberts, White, et al., 2012).

### 1.2. Epeirogeny and the Role of Dynamic Support

More popular models invoke the development of positive and negative mantle buoyancy anomalies generated by hot upwellings and subducting slabs to generate vertical motions (e.g., Humphreys, 1995; Karlstrom et al., 2012; Liu & Gurnis, 2010; Spencer, 1996; Thompson & Zoback, 1979). The admittance,  $Z$ , between long-wavelength ( $\gtrsim 800$ – $2,500$  km) free-air gravity anomalies and topography for western North America show that it has an elastic thickness of  $12\pm 3$  km, which implies that subplate buoyancy anomalies ought to measurably deflect the Earth's surface (McKenzie, 2003). At the longest wavelengths,  $Z=23\pm 5$  mGal/km, which suggests that the topographies of western North America, the Yukon, Central Mexico, and the Appalachian mountains are at least partially supported by subplate processes (e.g., Roberts, White, et al., 2012; Stephenson et al., 2014; Figure 1b). These locations of inferred subplate support are corroborated by seismic tomographic imaging, which shows that the upper mantle beneath these parts of North America is anomalously slow and juxtaposed against a central region with thick (>150 km) lithosphere (e.g., French et al., 2013; Molnar et al., 2015; Priestley & McKenzie, 2006; Ritsema et al., 2011; Rowley et al., 2013). Basaltic magmatism coincides with many of these low-velocity zones (e.g., Figure 2). Beneath western North America, an overall increase in melt volume at 40 Ma, as well as an abrupt change from lithospheric to asthenospheric signatures at 5 Ma, points toward the emplacement of anomalously hot material during the last 70 Ma (e.g., Fitton et al., 1991; Klocking et al., 2018; Roy et al., 2009; Figure 3). Drainage patterns of the four most prominent topographic swells (e.g., Yukon, western North America, Mexico, and Appalachians) are broadly radial, which suggests domal support of the present-day landscape (Figure 1b).

A burgeoning number of geodynamic models have been used to predict mantle flow patterns beneath the continent with a view to constraining the history of dynamic topography (e.g., Dávila & Lithgow-Bertelloni, 2015; Lithgow-Bertelloni & Gurnis, 1997; Liu et al., 2008; Mitrovica et al., 1989; Spasojević & Gurnis, 2012). These models estimate that transient dynamic topography has amplitudes of up to  $\pm 2$  km and wavelengths of hundreds to thousands of kilometers (see, e.g., Flament et al., 2015). They have been used to account for the aerial extent of the Western Interior Seaway as well as for Mesozoic-Cenozoic uplift, subsidence and magmatic patterns (e.g., Flament et al., 2015; Heller & Liu, 2016; Liu, 2015; Rowley et al.,

2013). There is considerable debate about how best to parametrize and test these models, and it is notable that most of them fail to match the power spectral characteristics of a global database of oceanic residual depth measurements (Hoggard et al., 2016). Thus, reliable histories of continental-scale vertical motions of the lithosphere are important constraints for this rapidly evolving field.

The purpose of this study is to develop a testable history of uplift and denudation for the North American continent. First, we review published estimates of rock and surface uplift and denudation used to constrain North American topographic growth since Campanian times. We then fill in some of the gaps and omissions by exploiting regional uplift measurements obtained from stratigraphic and biostratigraphic inventories. We generate a continent-wide history of regional rock uplift by inverting an inventory of 4,161 river profiles. The calculated rock uplift history is tested using independent stratigraphic data. Finally, we use this uplift rate history to carry out continental-scale landscape simulations whose predictions are tested using a combination of legacy thermochronometric and detrital zircon measurements.

## 2. General Stratigraphic Constraints

### 2.1. Birth of the Western Interior Seaway

The chronology of deformed igneous rocks, metamorphic time-temperature paths, low-temperature thermochronology, and biostratigraphic ages of deformed and overlapping sedimentary rocks testify to the existence of an orogenic belt that has spanned the length of the North American continent since Late Jurassic times (see, e.g., DeCelles, 2004). Shortening along a ~200-km-wide and ~2,000-km-long structural belt that is oriented north-south manifests the Sevier orogen (Gans & Miller, 1983; Wernicke, 1992). Marine sedimentary rocks deposited within the adjacent Western Interior Seaway provide a useful datum against which Cenozoic uplift can be gauged (e.g., Sahagian, 1987; Ziegler et al., 1985). Field mapping, seismic data, and borehole penetrations imply that up to 4 km of Late Jurassic to Late Cretaceous marine sedimentary rocks were deposited within the Western Interior basin, indicating that continental flooding was widespread (e.g., Niobrara Formation, Mancos Shale; Cross, 1986; DeCelles, 1994; Nassichuk & McIntyre, 1995; Roberts & Kirschbaum, 1995; Setterholm, 1994; Smith et al., 1994). These rocks have extensively documented ammonite biozones and known chronostratigraphy (e.g., Jeletzky, 1971; Kauffman & Caldwell, 1993; Obradovich & Cobban, 1975). Sedimentary isopachs and backstripped subsidence curves show that between ~92 and 82 Ma the Western Interior basin was narrow and that subsidence patterns are consistent with the growth of foreland basins generated by loading associated with the Sevier orogeny (Cross & Pilger, 1978; Cross, 1986; Heller & Liu, 2016; Pang & Nummedal, 1995; Roberts & Kirschbaum, 1995). In contrast, subsidence between ~80 and 67 Ma occurred over a broader region centered on Colorado and Wyoming. Loading by the Sevier belt or changes in sea level cannot easily account for either the lateral extent or amplitude of observed subsidence (Bond, 1976; Liu & Nummedal, 2004; Pang & Nummedal, 1995). A range of geodynamic models have been proposed to explain these subsidence patterns by invoking kilometer-scale Cretaceous dynamic drawdown of large parts of the continent (e.g., Gurnis, 1993; Liu et al., 2008; Mitrovica et al., 1989).

### 2.2. Regression of Western Interior Seaway

By ~70 Ma, when peak metamorphism became manifest within the main fold belt, eastward migration of thrust faulting resulted in an increasing partitioning of the Western Interior basin into smaller basins flanked by basement-cored uplifts (Cross, 1986; DeCelles, 2004; Dickinson et al., 1988; Stone, 1993). This “Laramide” structural style developed over a wide region east of the Sevier belt (DeCelles, 2004; Dickinson & Snyder, 1978). Despite the structural relief across these thrusts, intrabasinal deformation is insufficient to denude existing sedimentary deposits or to halt accumulation of Late Cretaceous marine sequences and associated deltaic facies (e.g., Dickinson et al., 1988). At the same time, a Late Cretaceous to Early Paleocene transition from marine deposition (e.g., Pierre shale and Lewis shale) to deltaic (e.g., Fox Hills sandstone) to terrestrial deposition (e.g., Lance formation) facies occurred diachronously across North America (Dickinson et al., 1988; Heller & Liu, 2016; Lillegraven & Ostresh, 1988; Setterholm, 1994). Paleoflow directions of conglomerates from the Laramide intramontane foreland basins (e.g., Paleocene Ohio Creek Conglomerate, Colorado; Maastrichtian-Paleocene Ojo Alamo Sandstone, New Mexico) indicate that a regional eastward tilt probably existed at ~70–60 Ma (Heller et al., 2013). Late Paleocene to Early Eocene terrestrial, synorogenic conglomerates deposited within the Middle Rocky

Mountains record active thrust faulting and erosion (Fan & Carrapa, 2014). These combined observations show that during Late Mesozoic to Early Cenozoic times the Western Interior Seaway retreated and substantial parts of western North America were uplifted (Dickinson et al., 1988; Roberts & Kirschbaum, 1995). The resultant facies change caused by retreat of this seaway has been linked with variable sedimentary flux, changing styles of subduction, hydration of the lower crust, and dynamic support (e.g., Dávila & Lithgow-Bertelloni, 2015; Humphreys et al., 2003; Kauffman & Caldwell, 1993; Levandowski et al., 2018). During this period, minor tectonic shortening occurred across the Colorado Plateau (Spencer, 1996).

### 2.3. Post-Cretaceous Events

Thermochronometric and incision rate histories suggest that Cenozoic denudation of the Colorado and Rocky Mountains plateaus occurred in several stages (e.g., Flowers et al., 2008; Karlstrom et al., 2017; Winn et al., 2017). Staged Cenozoic uplift and denudation of North America is consistent with the history of sedimentary deposition observed along the northern and western margin of the Gulf of Mexico (Galloway et al., 2000; Stephenson et al., 2014). Feng et al. (1994), Peel et al. (1995) and Galloway (2008) showed that Mesozoic strata in the Gulf of Mexico are relatively uniform in thickness, while Cenozoic sedimentary strata increase in thickness toward the west. The highest rates of sedimentary flux occurred during Paleocene (~65 Ma), Oligo-Miocene (~40–15 Ma) and Plio-Pleistocene (~5–0 Ma) times (Galloway et al., 2011). Timing of these depositional phases is broadly coeval with the history of uplift estimated from clumped isotopes ( $\Delta_{47}$ ) and with other paleoaltimetric proxies, which imply that the Colorado Plateau had an elevation of 1–2 km between Cretaceous and Oligocene times (e.g., Gregory & Chase, 1992; Huntington et al., 2010; Wolfe et al., 1998). Galloway et al. (2011), Blum and Pecha (2014), and Blum et al. (2017) argue that large-scale drainage of the Cordilleran highlands toward the Gulf of Mexico existed by at least Late Paleocene times and that drainage catchments probably extended up to the western flank of the Appalachian mountains. Further west, Cather et al. (2008) identified a major denudation event within the Colorado Plateau between the deposition of the Chuska Erg (35–27 Ma) and the Bidahochi Formation (~16 Ma).

Geologic mapping and regional palinspastic reconstructions suggest that the final stages of terrane accretion in Western Canada and Alaska occurred between ~50 and 40 Ma and in the Pacific Northwest after ~30 Ma, establishing the present-day tectonic configuration of the northwest Cordillera (Dickinson, 2004; Johnston, 2001). Oxygen isotope paleoaltimetry has been used to suggest that a kilometer-scale “Nevadaplano” plateau was present in British Columbia by ~50 Ma and that it migrated south toward Nevada by ~30 Ma (Chamberlain et al., 2012). The presence of an elevated, but low-relief, plateau is corroborated by reconstruction of deeply incised, west flowing paleovalleys across the present-day crest of the Sierra Nevada (Best et al., 2009; Cassel et al., 2009; Henry et al., 2012). Crosscutting relationships of extrusive magmatism and ignimbritic flows, and thermochronology together with wide-spread deposition of syntectonic basin fill suggest that regional compressive stress gave way to extension stress. The Basin and Range Province started to extend at ~30 Ma and experienced rapid Miocene (~20–15 Ma) stretching and subsidence, coeval with eruption of the Columbia River basalts (Cassel et al., 2009; Chamberlain et al., 2012; Colgan & Henry, 2009; Zoback et al., 1981).

The history and chemistry of extrusive western North American magmatism suggest that Cenozoic uplift is related to decompression melting of anomalously warm asthenosphere (Figure 2c; Ferrari et al., 2012; Fitton et al., 1991; Roy et al., 2009; Snyder et al., 1976). The NAVDAT database contains 6,713 samples of extrusive magmatism from the Colorado Plateau that suggest a trimodal history with peaks at ~70–55, 40–20, and 6–0 Ma (Figure 3a). Spatiotemporal patterns of magmatism record a westward migration, culminating in a maximum aerial extent during Oligocene times (Chapin et al., 2004). These phases of magmatism are broadly coeval with pulses of sedimentary flux within the Gulf of Mexico between ~60–50, 37–11, and 2–0 Ma (Galloway et al., 2011; Figure 3c). Recent correlation of basalt geochemistry with shear wave velocities suggests that magmatism and uplift of western North America is generated by a thermal anomaly, which sits beneath thin lithosphere (Klocking et al., 2018).

Mexican topography is characterized by an Altiplano-style physiography so that the 1–3 km high Sierra Madre Occidental, the Mexican Altiplano, the Trans-Mexican Volcanic Belt, and the Sierra Madre del Sur together form a broad, elevated region (Figure 1a). Reconstruction of an ignimbrite-capped plateau records up to 2 km of incision of the western highlands since 26 Ma (Montgomery & López-Blanco, 2003). The

southern portion of this region has peaks that are higher than 5 km. Oligocene ignimbrite flare-ups occurred throughout the Sierra del Sur and migrated southward during Miocene times with a decreasing lithospheric signature (Figures 2a and 2b; Ferrari et al., 1999; Ferrari et al., 2002; Ferrari & Bryan, 2007; Marquez et al., 1999). Thermal modeling of heat flow measurements suggests that anomalously hot mantle sits beneath the lithospheric plate (Ferrari et al., 2012).

The cratonic interior of North America, including the Canadian Shield, has a modest average elevation ( $\lesssim 0.5$  km; Figure 1a). Backstripping of sedimentary rocks recorded in boreholes shows that it has experienced slow ( $\sim 0.01$ – $0.001$  mm/a) Paleozoic subsidence (Armitage & Allen, 2010). Nonetheless, portions of the Canadian Rockies and of the craton show evidence of youthful uplift. Kimberlites of the Lac de Gras field in central Slave Craton that are  $\sim 75$ - to 45-Ma crop out at 550- to 600-m elevation. Significantly, these deposits contain xenoliths of marine and terrestrial sedimentary rocks of Albian ( $\sim 113$ – $100$  Ma) and Eocene ( $\sim 56$ – $45$  Ma) ages, respectively. The present-day absence of cratonic Phanerozoic sedimentary cover suggests that moderate ( $\geq 300$  m) uplift and denudation occurred prior to, and after, magmatic emplacement (Ault et al., 2013; Heaman et al., 2004; Nassichuk & McIntyre, 1995). Variations in coal rank from the Upper Cretaceous Plains of Alberta suggest that between 1.1 and 1.9 km of overburden was removed from the Western Canada basin within the last  $\sim 60$  Ma (Bustin, 1991; Nurkowski, 1984). These observations are in agreement with modeling of (U-Th)/He in Apatite (A-He) from the Slave craton, which indicate that regions surrounding the cratonic core of North America experienced diachronous post-Cretaceous uplift and exhumation with wavelengths of tens to thousands of kilometers (Flowers et al., 2012; Ault et al., 2013).

The origin of kilometer-scale Appalachian topography remains enigmatic. After the end of rifting at  $\sim 175$  Ma, the eastern seaboard constituted a passive margin (e.g., Klitgord et al., 1988). Long-term slow exhumation rates (20 m/Ma for  $>80$  Ma) inferred from apatite fission track (AFT) measurements are comparable to rates of fluvial erosion estimated using cosmogenic dating. These measurements have been interpreted as evidence for slow and steady decay of an old orogen (cf. Boettcher & Milliken, 1994; Matmon et al., 2003; Naeser et al., 2004; Pavich et al., 1985; Portenga et al., 2013). In contrast, A-He thermochronometry suggests that kilometer-scale Late Cretaceous denudation of the southern and northern Appalachians has occurred (Amidon et al., 2016; McKeon et al., 2014). Topographic relief of the crests of the Appalachian mountains has no obvious relationship to the underlying geologic terranes, which implies that prior tectonic shortening may not be the primary geomorphic control (McKeon et al., 2014).

#### 2.4. Neogene Uplift and Denudation

A range of observations suggest that the Appalachian Mountains experienced Neogene uplift and denudation. Elevation of the warped Orangeburg-Chippenham-Thornburg escarpments and of other reconstructed Cenozoic paleoshorelines record tens of meters of Pliocene to Recent uplift (Rowley et al., 2013; Spasojević & Gurnis, 2012). The shapes of longitudinal river profiles from the southern and central Appalachian Mountains are convex upward, which suggests that this landscape is disequilibrated (Gallen et al., 2013; Gallen, 2018; Miller et al., 2013; Prince & Spotila, 2013). Significantly, the Cenozoic stratigraphic record from the adjacent Atlantic shelf shows major pulses of Cretaceous and Miocene sedimentary flux (Pazzaglia & Brandon, 1996; Poag & Sevon, 1989). Sedimentary flux estimates are incompatible with slow and steady erosion of the Appalachian Mountains. Thermal modeling of A-He observations show increased Miocene exhumation of this region, which correlates with increased sedimentary flux (McKeon et al., 2014). As Taylor and Fitzgerald (2011) and McKeon et al. (2014) point out, the lack of post-Cretaceous AFT or A-He ages at other sites does not necessarily preclude Miocene uplift but it does imply that the magnitude of this denudation is small ( $\lesssim 1$  km). In Florida, coarse siliciclastic rocks with a Southern Appalachian provenance overlie Late Miocene carbonate platforms, an observation that is consistent with post-Miocene denudation (Missimer & Maliva, 2017). Detrital zircon analyses from the Atlantic Coastal Plain suggest that the recent erosion in the Appalachian Mountains is related to westward migration of eastern drainage divides (Naeser et al., 2016). These combined observations indicate that Appalachian physiography is not solely a result of erosional decay of a Paleozoic mountain chain (cf. Baldwin et al., 2003).

Youthful uplift of the northern Appalachian Mountains and of Newfoundland has also occurred. A combination of AFT modeling and  $^{40}\text{Ar}/^{39}\text{Ar}$  ages from Mount Washington in New Hampshire indicates an increased exhumation rate after 60 Ma (Amidon et al., 2016; Roden-Tice et al., 2012). Along the continental margin of Labrador, calibrated seismic profiles show that Mesozoic strata dip seaward and are truncated by

Late Oligocene and younger strata, which are consistent with phases of regional uplift (Dickie et al., 2011). A regional Miocene unconformity has also been documented in offshore seismic data (Ainsworth et al., 2014). Subsidence curves and vitrinite reflectance measurements from the Hopedale E-33 well offshore Labrador show that pre-Pliocene strata have been more deeply buried by as much as 750 m prior to removal of Miocene strata (Japsen et al., 2016). Earthquake tomographic modeling has identified a region of slow velocity, which has a diameter of ~400 km and is known as the Northern Appalachian Anomaly (Menke et al., 2016). This anomaly occurs within the asthenosphere beneath southern New England, and, if it is of thermal origin, it may play a role in generating youthful uplift.

In western North America, sedimentary deposits of the Ogallala Group are exposed in the Great Plains and suggest that the eastern margin of the Colorado Plateau was regionally tilted during Miocene times (McMillan et al., 2002). Stratigraphic constraints on the timing of regional tilting places this differential uplift between ~6 and 3.7 Ma (Duller et al., 2012). Evidence for younger (i.e., post-8 Ma) regional uplift and surface tilting is corroborated by differential incision of the Rocky Mountains and by a reconstructed low-relief surface generated by post-Laramide basin fill, which reached as far east as the Great Plains (McKenna & Love, 1972; McMillan et al., 2006). Incision histories of  $^{40}\text{Ar}/^{39}\text{Ar}$ -dated basaltic flows within the Colorado, Columbia, and Rio Grande catchments help to constrain long-term landscape development (e.g., Karlstrom et al., 2008, 2017; Wakabayashi & Sawyer, 2001). These catchments have been incised by tens to hundreds of meters during Neogene times (e.g., Channer et al., 2015; Karlstrom et al., 2012; Nereson et al., 2013; Repasch et al., 2017).  $^{40}\text{Ar}/^{39}\text{Ar}$  dating and magnetostratigraphy of tephra deposits within the oldest marine deposits of the Gulf of California suggests that rifting of the Gulf of California initiated by ~7 Ma. Present-day elevations (>300 m) of the shallow marine Upper Bouse formation implies that uplift of the lower reaches of the Colorado River occurred after ~4.8 Ma (Dorsey et al., 2018). Quaternary marine terraces along southwestern and eastern coasts of Mexico are elevated by several tens of meters above sea level, an observation that is interpreted as a consequence of uplift at rates of up to 3 m/ka (Ramirez-Herrera et al., 2011; Self, 1977).

### 3. Uplift Histories Inferred From Sedimentary Strata

Elevation of dated marine sedimentary strata is probably the least contentious and most robust constraint on the history of continental uplift. In North America, the distribution of Cretaceous marine rocks, notably the Mancos Shale, provides excellent evidence for kilometer-scale uplift of the Colorado-Columbia-Rocky Mountains plateaus since ~80 Ma (e.g., Roberts & Kirschbaum, 1995; Sahagian, 1987; Ziegler et al., 1985). Specifically, the youngest outcropping marine to terrestrial sedimentary sequences, which mark the latest regressive transitions, provide the key datum against which uplift can be measured.

To determine cumulative uplift histories at spot locations across North America, we exploit an inventory of 4,633 unique marine fossil assemblages that have been extracted from the Paleobiology Database (PBDB, <https://paleobiodb.org>). This inventory is focused upon Late Cretaceous and Cenozoic samples, which span the last 82 Ma. The PBDB is a substantial, collection-based, occurrence and taxonomic data set of biota that also contains information about host rock lithology, stratigraphy, age, and paleoenvironmental setting. Figure 4a shows the locations of samples exploited in this study. Additional stratigraphic constraints for the timing of uplift initiation were compiled using the methodology of Dickinson et al. (1988), which identifies the last marine to nonmarine transitions in the sedimentary record. Each regressive sequence is identified from published facies interpretations (e.g., Gani et al., 2015; Johnson et al., 2002; Roberts & Kirschbaum, 1995). Locations were determined from state geologic maps (<https://ngmdb.usgs.gov>; Figure 4a). Particular care was taken to identify the lateral and temporal variability of marine to terrestrial transitions, such as those observed for depositional sequences within the Star Point Sandstone, Blackhawk, Castlegate, and Sego Sandstone Formations (e.g., Gani et al., 2015). Stratigraphic ages were assigned using published biostratigraphic and chronostratigraphic sections for the Western Interior Seaway (Merewether & McKinney, 2015; Obradovich & Cobban, 1975, Figure 4b). The PBDB provides additional constraints for loci of Late Cretaceous paleocoastlines, which themselves provide a reference paleogeography against which regional uplift can be gauged (Cao et al., 2017; Kauffman & Caldwell, 1993; Roberts & Kirschbaum, 1995; Sahagian, 1987; Smith et al., 1994; Figure 4b).

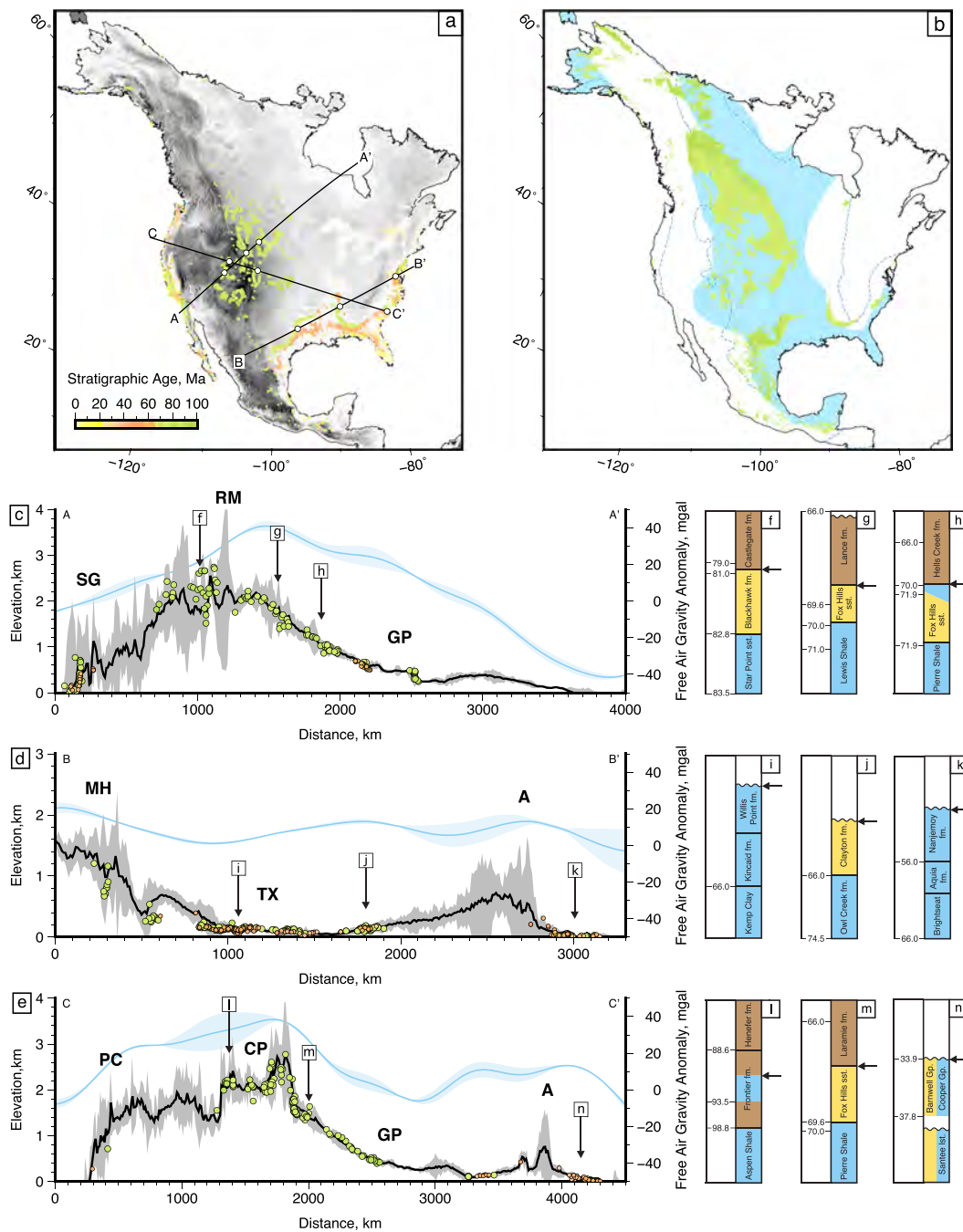


**Figure 4.** Stratigraphic and biostratigraphic constraints. (a) Colored circles show location and age of marine fossil assemblages from Paleobiology database (PBDB paleobiodb.org) as well as youngest marine to nonmarine stratigraphic transitions (Dickinson et al., 1988). Black lines = locations of vertical cross sections shown in panels (c)–(e); white circles = locations of stratigraphic columns shown in panels (f)–(h), (i)–(k), and (l)–(n). (b) Extent of Late Cretaceous seaway interpreted from PBDB. Solid blue polygons/dashed lines = maximum flooding extent of Cretaceous (i.e., Late Maastrichtian) interior seaway (Smith et al., 1994; Kauffman & Caldwell, 1993). Dark/light green polygons = outcropping Lower/Upper Cretaceous rocks (Reed et al., 2005). (c–e) Topographic and stratigraphic cross sections (see panel a for location); black line with gray band = topography  $\pm$  maximum and minimum elevation within 100-km swath; labeled arrows = location of stratigraphic columns shown in adjacent panels; colored circles = biostratigraphically dated marine rock colored according to age (see scale bar); light blue band = free-air gravity anomaly  $\pm$  maximum and minimum within 100-km swath from GRACE database (Figure 1). SG = San Gabriel Mountains; RM = Rocky Mountains; GP = Great Plains; MH = Mexican Highlands; TX = Texas; A = Appalachian Highlands; PC = Pacific Coast Ranges; CP = Colorado Plateau. (f–n) Generalized stratigraphic sections with youngest marine regression or outcropping marine strata (arrow); blue boxes = shallow marine facies; yellow boxes = marginal marine/shoreface facies; brown boxes = terrestrial facies.

**Table 1**  
*Biostratigraphic Constraints on Uplift Histories Adapted From Five Samples in the PBDB*

Province	Latitude	Longitude	Elevation (m)	Fossil	Age (Ma)	Formation	PWD (m)	$\bar{U}$ (mm/a)
CP	38.9017	-107.9258	1,593	<i>Baculites aquilaensis</i>	77.05 ± 6.45	Mancos Shale	20–200	0.0258 ± 0.00289
RM	40.3166	-107.0333	2,310	<i>Trochocyathus egerius</i>	69.05 ± 3.05	Lewis Shale	0–20	0.0336 ± 0.00179
GP	43.2694	-104.2716	1,213	<i>Baculites baculus</i>	69.05 ± 3.05	Pierre Shale	15–40	0.0179 ± 0.0013
AP	38.8719	-78.5136	283	<i>Myliobatis dixoni</i>	61.0 ± 4.0	Nanjemoy	0–100	0.00546 ± 0.00184
MX	28.2333	-100.2166	203	<i>Sphenodus aberrans</i>	68.3 ± 2.3	Escondido	0–50	0.00335 ± 0.00123

Note. CP = Colorado Plateau; RM = Rocky Mountains; GP = Great Plains; AP = Appalachian Mountains; MX = Mexico; latitude/longitude given in decimal degrees; PWD = paleowater depth;  $\bar{U}$  = average uplift rate (see text). Supporting information provides detailed fossil occurrences and uplift rate estimates for complete inventory.

At any given location, cumulative uplift,  $\int U dt$ , is equal to  $z + P \pm S$ , where  $U$  is uplift rate,  $t$  is age,  $z$  is present-day elevation,  $P$  is paleowater depth and  $S$  is paleo-sea level with respect to present-day mean sea level. Calculated uplift  $U$  is both rock and surface uplift and is a minimum value, since any putative subsidence that occurred after deposition cannot easily be determined. Elevation of each sample was extracted from the Advanced Space-borne Thermal Emission and Reflection Radiometer (ASTER) global digital elevation model (GDEM), which has vertical and horizontal resolutions of ~20 and ~75 m, respectively (Tachikawa et al., 2011). In each case, elevations are based upon locations reported in the PBDB, which have accuracies of ±0.01°, which is equivalent to ±1 km. The greatest source of uncertainty is paleobathymetry. Paleowater depth ranges were provided for some samples in the database, based on the presence of depth-specific marine fauna (e.g., benthic foraminifera) and indicative sedimentary bedforms. In most cases, paleobathymetry was estimated from the reported environment of deposition and calibrated from marine faunal occurrences (e.g., dinoflagellate cysts and benthic foraminifera), and from geologic descriptions of the formation. The paleobathymetric template described by Immenhauser (2009) was assumed (e.g., neritic: 0–150 m; upper bathyal: 150–500 m; middle bathyal: 500–2000 m). Obviously, deltaic and marginal marine deposits have much smaller uncertainties and therefore usually yield better constrained uplift histories. Examples of the biota we used are shown in Table 1 and a comprehensive inventory is provided in the supporting information.

Stratigraphic observations of the last marine regression provide the tightest constraints for paleobathymetry since they record the last time the reference surface sat at sea level, for which the paleowater depth is effectively zero with minimal uncertainty. Many stratigraphic sequences are temporally well defined by ammonite biostratigraphy with uncertainties of ±0.1 Ma. Figures 4f–4n show examples of stratigraphic columns used to estimate regional uplift (supporting information). Glacio-eustasy during Late Cretaceous and Paleogene times is not accurately constrained, and so we included sea level change as an additional uncertainty,  $\delta S = \pm 50$  m. This uncertainty is probably appropriate for post-Campanian sea level variations (Miller, 2005). Since all of the stratigraphic and biostratigraphic samples crop out at the Earth's surface, a loading correction for overlying strata is not required (Sahagian, 1987). Extremal uncertainties in elevation, paleowater depth, sea level, and sample age were used to estimate uncertainties of average uplift rates,  $\bar{U}$ , such that

$$\begin{aligned}\bar{U}_{\max} &= (P_{\max} + Z_{\max} + S_{\max})/a_{\min}, \\ \bar{U}_{\min} &= (P_{\min} + Z_{\min} + S_{\min})/a_{\max}.\end{aligned}\quad (1)$$

Sample age,  $a$ , has a range which primarily depends upon the first and last occurrences of the faunal assemblage in question (Gradstein et al., 2012).

Compiled uplift constraints are summarized in Figures 4 and 5. Cross sections shown in Figures 4c–4e compare present-day elevations of biostratigraphic and stratigraphic constraints with a 100-km-wide topographic swath along three key transects. In each case, the spatial distribution of samples reveals a broad swell, which matches the topography. Figure 5 shows the interpreted paleowater depth and calculated uplift, which is greater than present-day elevation. Samples used in this study indicate that water depth of the Late Cretaceous Western Interior Seaway was ≤300 m (Figure 5a; Arthur & Sageman, 2004). These shallow

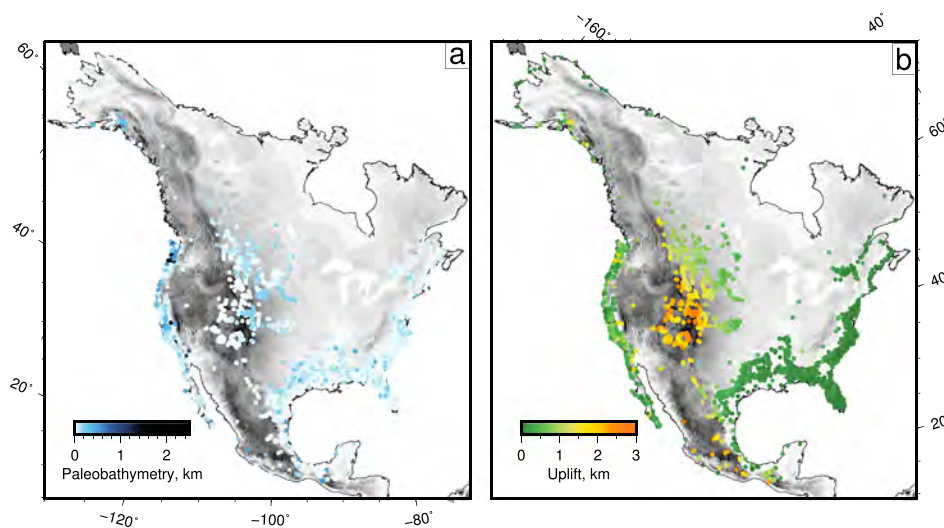


**Figure 5.** Paleobathymetry and cumulative uplift from stratigraphic and biostratigraphic constraints. (a) Blue circles = paleowater depths (see scale bar). (b) Colored circles = cumulative uplift determined from marine to terrestrial transitions recorded by stratigraphic record and fossil assemblages.

values imply that the present-day elevation of each sample is broadly representative of its cumulative uplift. Our compiled results show that since 80–65 Ma, a region encompassing the Colorado Plateau, Southern Rocky Mountains, and swathes of the Great Plains have been uplifted to form a broad swell that has a wavelength of ~1,500 km (Figures 4c, 4e, and 5b). Calculated uplift reaches a maximum of ~3 km in the Colorado Plateau and Southern Rocky Mountains, decreasing smoothly to ~500 m at the eastern edge of the Great Plains (e.g., Figure 5). The age constraint for initiation of uplift is in general agreement with the proposed start of the Laramide orogeny (Dickinson et al., 1988). Superimposed on this broad swell are shorter wavelength (<100 km) variations in elevation of up to 1 km, which probably reflect uplift caused by horizontal shortening within the Rocky Mountains (Figures 4c and 4e; e.g., Fan & Carrapa, 2014). In general, however, the correlation between large-scale uplift patterns and individual Laramide structures is tenuous since in many locations there is little difference in cumulative uplift between the Rocky Mountain front and the Great Plains (cf. DeCelles, 2004; Figure 5b). A similar pattern is observed for the central and southern portions of the Mexican Highlands where 1.5–2.5 km of post-Cretaceous uplift decreases smoothly toward the Gulf coast and toward the Basin and Range province. Sample density makes it difficult to distinguish smaller scale uplift patterns.

Along the Gulf and Atlantic Coastal Plains, sedimentary successions containing marine fossils were deposited on a shallow marine shelf, at the shoreface, or within a deltaic environment. In general, they record seaward progradation of the continental shelf (Figure 5a; Gohn, 1988; Olsson et al., 1988; Pazzaglia & Gardner, 1994). Figure 4d shows Late Cretaceous to Eocene age samples from the Gulf Plain region at elevations of ~200 m. Here, calculated uplift smoothly increases westward toward the Mexican Highlands where Cretaceous samples from the Rio Grande Embayment are at an elevation of 500 m. Regional tilt of the eastern Gulf Coast and Atlantic Coastal Plain samples (Figures 4d and 4e; stratigraphic columns j, k, and n) is suggestive of long-wavelength (~1,000 km) surface uplift of magnitude  $\leq 300$  m that has developed since Eocene times. Regional uplift calculated for samples along the Pacific Coastal Ranges reveals no simple large-scale pattern, which probably reflects the complex tectonic history of terrane accretion, lateral displacement, subduction, and subsidence (e.g., Awater, 1970).

The magnitude of regional uplift across the Colorado Plateau, Mexico, and the Appalachian Mountains is obviously too great to be accounted for by glacio-eustasy (cf. Miller, 2005). Figures 4c–4e shows the pattern of maximum and minimum free-air gravity anomalies, which broadly mimics topographic elevation. Long-wavelength (>1,000 km) post-Cretaceous warping of North American topography and the colocation of gravity anomalies, slow shear wave velocity anomalies, and magmatic observations indicate that subplate support has played a significant role in generating and maintaining kilometer-scale Cenozoic epeirogeny

of large portions of North America (cf. Figures 1 and 2). Despite the spatial and temporal coverage provided by the PBDB, there are extensive tracts where uplift histories are poorly understood since it is difficult to interpolate between spot measurements. A potentially fruitful approach is to exploit drainage patterns, which are ubiquitous throughout the continent.

#### 4. Geomorphic Considerations

In principle, drainage networks should indirectly record uplift histories although this record is obscured by the erosional process (e.g., Howard, 1994; Kirby & Whipple, 2001; Snyder et al., 2000; Whipple & Tucker, 1999; Wobus et al., 2006). Significant effort has been put into developing techniques that can be used to extract information about geologic and geomorphological processes from fluvial networks. Many modeling studies have shown that the shape of a river profile is affected by changes in uplift rate, which acts to generate transient knickzones (e.g., Crosby & Whipple, 2006; Howard & Kerby, 1983; Rosenbloom & Anderson, 1994). It is evident that longitudinal river profiles from multiple catchments share common knickzones, which suggests that uplift rate can affect whole catchments (e.g., Roberts, Paul, et al., 2012; Roberts et al., 2019). In this study, we apply a general inverse approach that enables regional rock uplift rates as a function of time and space to be extracted from large inventories of river profiles (Rudge et al., 2015). This approach has four important steps. First, continent-wide drainage patterns are extracted from a suitable digital elevation model and their veracity checked using satellite imagery. Second, a physically appropriate erosional model is chosen. Third, the erosional constants used in this model are calibrated and the drainage inventory is inverted to determine the smoothest rock uplift rate history that minimizes the misfit between observed and calculated river profiles. It is crucial that the calculated rock uplift history is carefully tested using independent geologic observations. Finally, the calibrated uplift rate history can be used to parameterize landscape evolution models that make testable predictions about regional denudation and sedimentary flux, which allows us to examine sensitivities of drainage planforms to calculated uplift. Each of these steps is tackled in the following way.

##### 4.1. Drainage Inventory

An inventory of 4,161 river profiles was extracted from the ASTER GDEM database. Rivers were extracted from cells with calculated upstream drainage areas larger than  $4 \text{ km}^2$ . Esri flow-routing algorithms were used to calculate overland flow, which in turn enables river profiles to be constructed. The planform drainage network was compared to satellite imagery (e.g., Copernicus, Landsat), and it can be shown that the extracted network has high fidelity in regions away from flat topography and narrow ( $<30 \text{ m}$  wide) gorges. Figure 1 b shows the drainage distribution for North America, which is radially distributed about four major topographic swells: the Yukon plateau (centered on  $60^\circ\text{N}$  and  $140^\circ\text{W}$ ), the Colorado-Columbia-Rocky Mountains plateaus ( $45^\circ\text{N}$  and  $-105^\circ\text{W}$ ); Mexico ( $20^\circ\text{N}$  and  $100^\circ\text{W}$ ); and the Appalachian mountains ( $35^\circ\text{N}$  and  $80^\circ\text{W}$ ).

Families of longitudinal river profiles grouped by catchment are shown in Figure 6. Profiles from the Colorado catchment exhibit two substantial convexities at  $\sim 500$ – $1,000 \text{ km}$  and at  $\sim 1,500$ – $2,500 \text{ km}$  (Figure 6). River profiles from the Columbia catchment and from the upper western reaches of the Mississippi catchment also have substantial knickzones (Figure 6). Pronounced convexities are observed on river profiles that drain northern and eastern North America (e.g., at  $\sim 1,500$ – $2,000 \text{ km}$  along the Nelson River). Many other North American catchments also have large convex-upward knickzones. The locations of these broad knickzones do not generally correlate with lithologic contacts, which suggests that their shapes are not related to substrate (e.g., bedrock) in a simple way (Roberts, White, et al., 2012). Instead, the observed commonalities of long-wavelength knickzones draining the four topographic swells suggests that they could have been generated by the spatial and temporal pattern of regional uplift.

##### 4.2. Erosional Parametrization

Shapes of longitudinal river profiles,  $z(x)$ , are controlled by the history of rock uplift rate,  $U$ , and by erosion rate,  $E$ , both of which can vary as a function of space,  $x$ , and time,  $t$  (e.g., Anderson & Anderson, 2010; Davis, 1899; Gilbert, 1877; Howard, 1994; Loget & Van Den Driessche, 2009; Sklar & Dietrich, 1998; Whipple & Tucker, 1999). A range of laboratory experiments and field measurements suggest that erosion rate depends upon a suite of complex processes that include the dynamics of water flow (e.g., discharge, turbulence, and

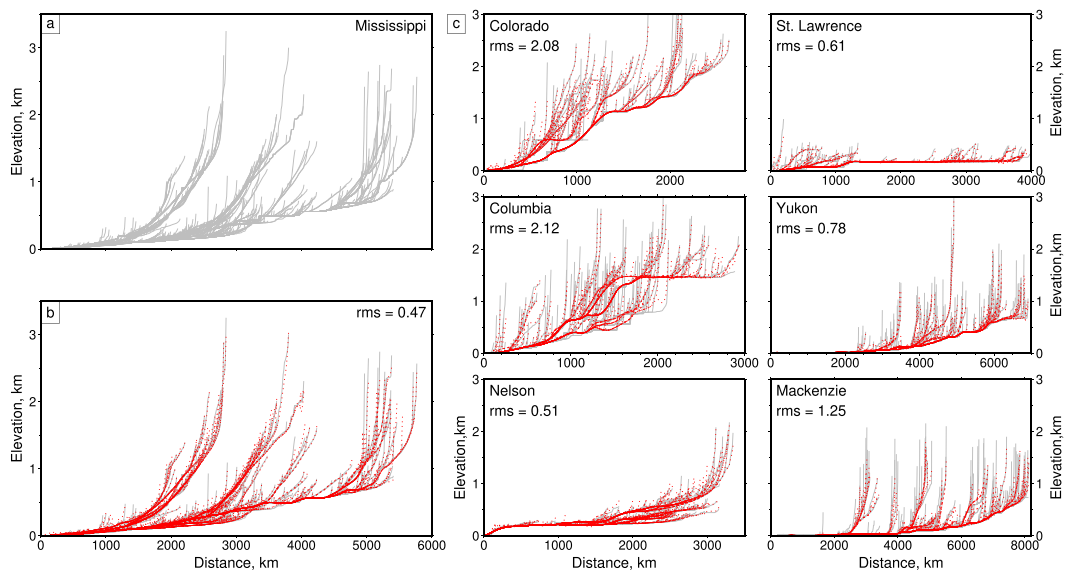


**Figure 6.** Inverted longitudinal river profiles. (a) Observed river profiles for Mississippi and its principal tributaries (see Figure 1). (b) Observed and calculated river profiles for Mississippi catchment. Red dotted lines = best fitting theoretical river profiles calculated using uplift history shown in Figure 8; value of root-mean-square (rms) misfit is shown in top right-hand corner. (c) Observed and calculated river profiles from six catchments shown in Figure 1.

vorticity), strength of the substrate (e.g., bedrock), orientation of jointing and fracturing, local erosional mechanisms, sediment supply, and biota (e.g., Allen et al., 2013; Baynes et al., 2018; Brocard et al., 2016; Brocard & Van Der Beek, 2006; Castellort et al., 2015; DiBiase et al., 2014; Mackey et al., 2014; Rengers & Tucker, 2014; Sklar & Dietrich, 1998, 2001).

At continental scales, it appears that large, coherent signals become emergent and that the stream power equation provides a practicable way to model drainage evolution through time and space (e.g., Roberts et al., 2019). For example, at wavelengths  $>10$  km, lithology does not appear to correlate with changes in slope, with curvature or with stream power (Roberts, White, et al., 2012; Czarnota et al., 2014). These inferences are consistent with spectral analyses of river profiles, which suggest that processes operating at long wavelengths ( $>100$  km) dominate the shapes of river profiles (Roberts et al., 2019; Roberts, 2019). Assumptions of erosional thresholds do not seem to be required in order to achieve a good match between observed and calculated river profiles at these long wavelengths (Roberts, White, et al., 2012). Furthermore, changes in precipitation rate where the period is less than about 1 Ma do not significantly affect calculated river profile shapes (e.g., Paul et al., 2014). Fluvial erosion appears to be a highly integrative process such that regional uplift primarily determines profile shape. The empirical stream power equation is given by

$$\frac{\partial z(x, t)}{\partial t} = -vA(x)^m \left( \frac{\partial z(x, t)}{\partial x} \right)^n + U(x, t), \quad (2)$$

where upstream drainage area  $A$  varies as a function of distance,  $x$ ;  $z$  is elevation above sea level,  $t$  is time, and  $U$  is rock uplift rate. Values of the erosional constants  $v$ ,  $m$ , and  $n$  can be determined by independent calibration. Equation (2) can be solved in order to calculate  $U$ . For example, Pritchard et al. (2009) demonstrated that  $U$  can be extracted from river profiles by exploiting the method of characteristics. Later, Royden and Perron (2013) employed the same integrative approach to calculate metrics that may relate to landscape evolution. These metrics, notably  $\tau_G$  and  $\chi$ , are often used to gauge the time taken for erosional signals to propagate through a given landscape and to infer drainage divide migration. A challenging problem is that regional uplift signals are generally inserted into the upstream reaches of individual rivers and catchments. An obvious solution is to pose the inverse problem whereby a smoothly varying rock uplift rate history,  $U(x, y, t)$ , is sought. The problem can be solved by either linear or nonlinear optimization. We assume that drainage area is temporally invariant, which implicitly assumes that reorganization of planform does not significantly affect shapes of rivers at the scales of interest (Paul et al., 2014; Rudge et al., 2015). Significantly, no a

priori assumptions about the spatial and temporal distribution of uplift signals are made. An inverse approach provides a pragmatic and testable way to calculate rock uplift rate histories at scales appropriate for investigating histories of subplate support.

#### 4.3. Inverse Modeling

The inverse scheme proposed by Pritchard et al. (2009) was generalized to incorporate “erosional diffusivity” and spatiotemporal changes in uplift rate histories by exploiting quasi-linear optimization methodologies (Roberts & White, 2010; Roberts, Paul, et al., 2012). A significant benefit of nonlinear inverse modeling is that it is possible to investigate the importance of erosional parameters whose values are much debated (Lague, 2014). For example, a suite of inverse models shows that residual misfit is minimized when the slope exponent,  $n$ , equals 1 (Paul et al., 2014). This result means that a simplified erosional model can be used to develop a linearized inverse model using a Bayesian approach in which a posteriori probability distributions (e.g., prior guesses at approximate rock uplift histories) are defined and, alternatively, a damped linear least squares approach that has a null starting set (Fox, Goren, et al., 2014; Goren et al., 2014; Rudge et al., 2015). Other schemes have also been proposed (e.g., Campforts & Grovers, 2015, Glotzbach, 2015).

Rudge et al. (2015) show that smooth spatiotemporal rock uplift histories can be obtained by linear inverse modeling without recourse to prior information. By solving the simplified stream power equation using the method of characteristics, the landscape response time,  $\tau_G$ , can be expressed as

$$\tau_G - t = \int_0^{x(t)} \frac{dx}{vA^m}. \quad (3)$$

Elevation is given by

$$z^* = \int_0^{\tau_G} U(x(t), t) dt, \quad (4)$$

(Luke, 1972; Weissel & Seidl, 1998). The resultant set of linear equations that relate elevation to rock uplift and erosion is rewritten in matrix form as

$$\mathbf{z} = \mathbf{M}\mathbf{U}. \quad (5)$$

Families of river profiles are inverted by minimizing

$$|\mathbf{M}\mathbf{U} - \mathbf{z}|^2 + \lambda_S^2 |\mathbf{S}\mathbf{U}|^2 + \lambda_T^2 |\mathbf{T}\mathbf{U}|^2. \quad (6)$$

where  $S$  and  $T$  are the spatial and temporal smoothing matrices, respectively (Rudge et al., 2015).  $U$  is permitted to vary subject to a non-negativity constraint,  $\mathbf{U} \geq 0$ , since river profile elevations constitute positive measurements. Uplift rate is allowed to vary as a function of time at vertices arranged in a triangular grid with a spacing of 125 km. The starting set is the null set, and we make no assumption about preexisting North American paleotopography. Uplift along river profiles is linearly interpolated from this spatiotemporal grid. It is important to note that the model cannot resolve uplift rate at times that are greater than the largest value of  $\tau_G$ . Following Parker's (1994) protocol, the spatial and temporal smoothing coefficients,  $\lambda_S$  and  $\lambda_T$ , are systematically varied to identify the smoothest model that yields the best fit between observed and calculated river profiles (Figure 7). Here, we used  $\lambda_S=0.5$  and  $\lambda_T=0$  and the effective temporal resolution is just under 6 Ma. Different values of  $\lambda_S$  and  $\lambda_T$  have also been tested.

One way to constrain the value of  $m$  is to calculate residual misfit from a suite of inverse models for which  $m$  is systematically varied. In each case, it is important to ensure that the same number of free parameters is used. In essence, this approach exploits the spatial geometry of drainage networks (i.e.,  $A(x)$ ) to constrain  $m$ . Crucially, we allow rock uplift to vary spatially and temporally, which means signals can be inserted at any position along different river profiles and we do not assume river profiles are in steady state (i.e.,  $\partial z / \partial t = 0$ ). Indeed, we caution against the use of methodologies, which assume steady state, which exploit the derivative of river profiles, or which prescribe an a priori uplift history. In general, all three of these assumptions yield unstable and misleading results. Figure 7 shows that North American river profiles are consistent with an optimal value of  $m=0.4$ , although the range  $0.2 \leq m \leq 0.5$  has sufficiently small residual misfits to be deemed acceptable. The value of  $v$ , which trades off against  $m$ , was calibrated using the history of incision

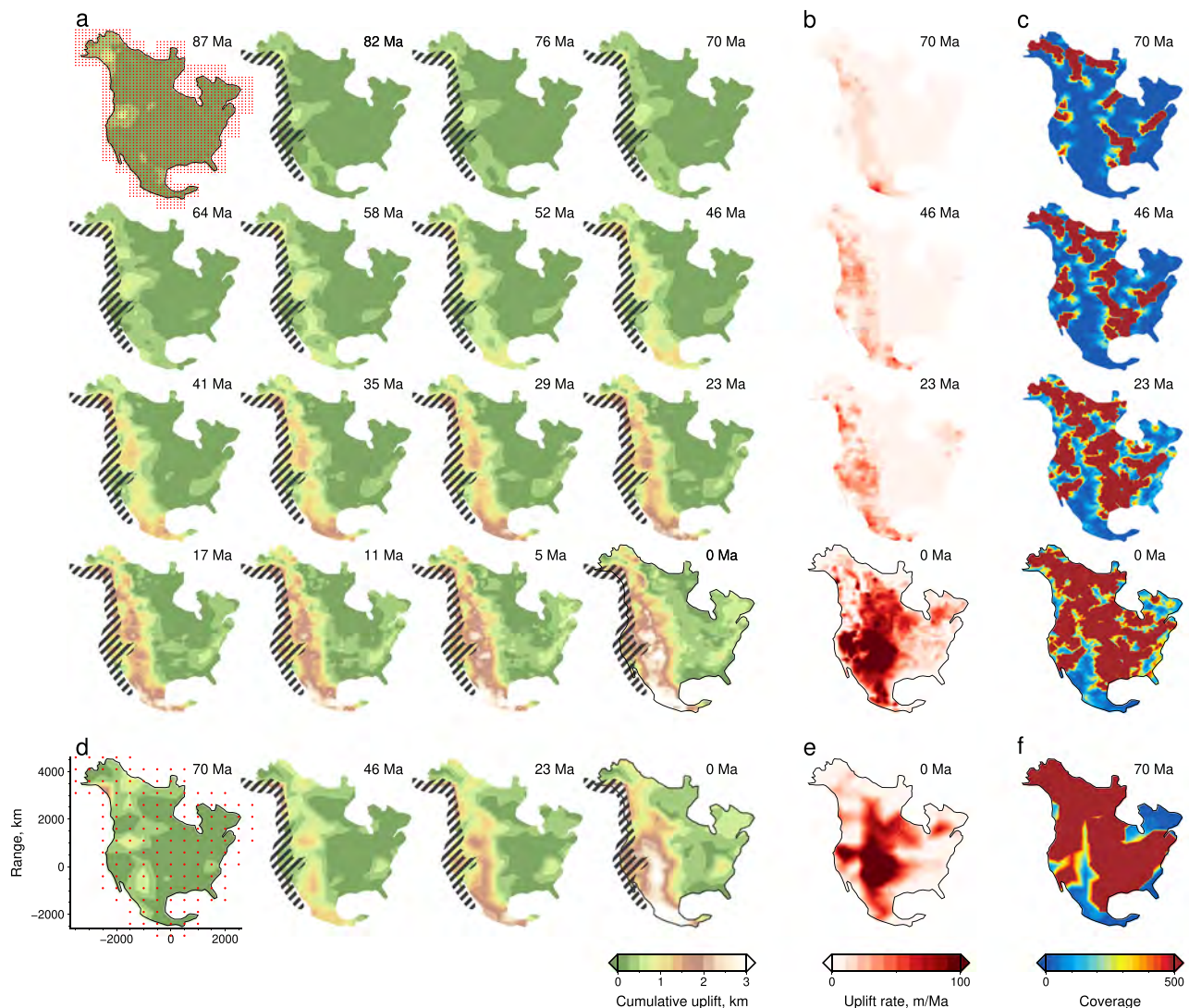


**Figure 7.** Inverse model parametrization. (a) Data misfit plotted as function of model smoothness for suite of inverse models with different values of smoothing parameter,  $\lambda_S$  (see Figure 8a for configuration of inverse model). Black arrow = locus of smoothest, best fitting model where  $\lambda_S = 0.5$ . (b) Residual misfit plotted as function of erosional parameter  $m$ . Black arrow = locus of weak global minimum at  $m \approx 0.4$ . (c) Cumulative model coverage as a function of time (Figure 8c). (d) Histogram of residual misfit between observed and predicted river profiles. (e) Inset showing full frequency distribution of residuals. (f) Residual positive misfit map between observed and calculated river profiles. (g) Residual negative misfit map.

recorded by eroded lava dams within the Grand Canyon (Karlstrom et al., 2008). The mean incision rate is  $111 \pm 7$  m/Myr. By combining this rate with local slope and area measurements Roberts, White et al. (2012) showed the relationship between erosional parameters  $v$  and  $m$  is  $v = 4.16 \times 10^4 \times (2.78 \times 10^{-12})^m$ . For  $m=0.4$ ,  $v$  has a value of  $0.99 \pm 0.062$  m<sup>0.2</sup>/Myr. We explore the impact of changing  $v$  by plus or minus 1 order of magnitude (supporting information).

The optimal fit between observed and calculated river profiles shown in Figure 6 is obtained using the cumulative rock uplift history shown in Figure 8. The root-mean-square (rms) misfit is given by

$$\left[ \frac{1}{N} \sum_{i=1}^N \left( \frac{z_i^o - z_i^c}{\sigma} \right)^2 \right]^{1/2}, \quad (7)$$

where  $N$  = number of data values and  $z^o$  and  $z^c$  are observed and calculated river elevations, respectively. Elevation variance was set as a constant value of  $\sigma=20$  m, based upon the reported resolution of the

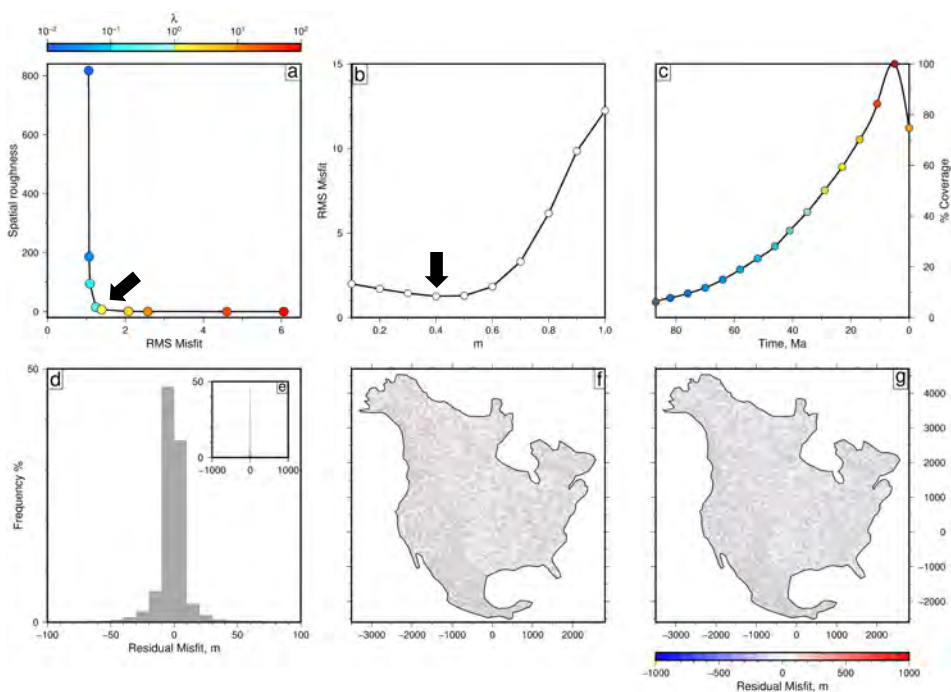


**Figure 8.** Calculated uplift history for North America. (a) Sixteen panels that show cumulative uplift history (i.e., temporally integrated uplift rate history) calculated by linear inverse modeling of 4,161 river profiles (residual rms misfit = 1.25; Figure 6). Grid of red points in top left-hand panel = loci of vertices used to discretize uplift rate. Age, in millions of years, is shown for each panel. Hatched region = Great Basin and Pacific margin where internal drainage, plate accretion, and strike-slip tectonics compromise assumptions that underpin inverse model. (b) Calculated uplift rate at four different times. (c) Selected panels at four different times that show model coverage (i.e., number of nonzero entries in model matrix, M, corresponding to given uplift node). Note that model coverage is highest toward present day and significantly decreases for ages >70 Ma (see Figure 7c). (d) Four panels showing cumulative uplift history of North America calculated using coarser mesh (residual rms misfit = 2.62). (e and f) Calculated uplift rates and model coverage for coarser mesh at 0 Ma. rms = root-mean-square.

ASTER database (Tachikawa et al., 2011). We emphasize that alternative objective functions can be used to measure the goodness of fit between observed and calculated river profiles without significantly affecting our principal results. Finally, we note that our approach does not explicitly address the difficult problems of internal drainage or of strike-slip tectonics, which means that calculated uplift histories along the Pacific seaboard and Great Basin should be treated with caution.

#### 4.4. Calculated Rock Uplift History

The calculated uplift history is shown in Figure 8. This history yields a residual rms misfit of 1.25 between observed and calculated river profiles. The most striking feature of this history is the Cenozoic growth of topography in western North America, which can be divided into two principal uplift events. Between ~80 and 40 Ma, regional uplift rate is modest, rarely exceeding ~0.02 mm/a. Between 30 and 20 Ma and the present day, uplift rate dramatically increases and reaches values as high as 0.1 mm/a. This calculated history predicts that the Colorado-Columbia-Rocky Mountains plateaus was uplifted from approximately sea level (i.e., <250 m) at ~80 Ma to an average elevation of 1.5–2.5 km at the present day. Note that the Rocky Mountains front and the Great Plains are uplifted at approximately the same time. Late Cretaceous to Recent cumulative uplift reaches 2.5–3.0 km within the southern Rocky Mountains, decreasing northward to ~1.5 km toward the Canadian Rockies and eastward to 0.5–1.0 km toward the Great Plains. Along the southern slopes between the Rocky Mountains and the Great Plains, cumulative uplift appears to have occurred in two broadly synchronous pulses between 60–40 and 20–0 Ma. Regional uplift is progressively younger and of shorter duration toward the north. The southern portion of the Great Plains becomes emergent after 20 Ma.

With the exception of the Rio Grande Embayment, calculated cumulative uplift along the Gulf Coastal Plain is <250 m. Between Georgia and the Mississippi Embayment, a rapid episode of regional uplift occurs at ~35 Ma. A cumulative uplift of 400 m is predicted to have occurred within the last 20 Ma for the Rio

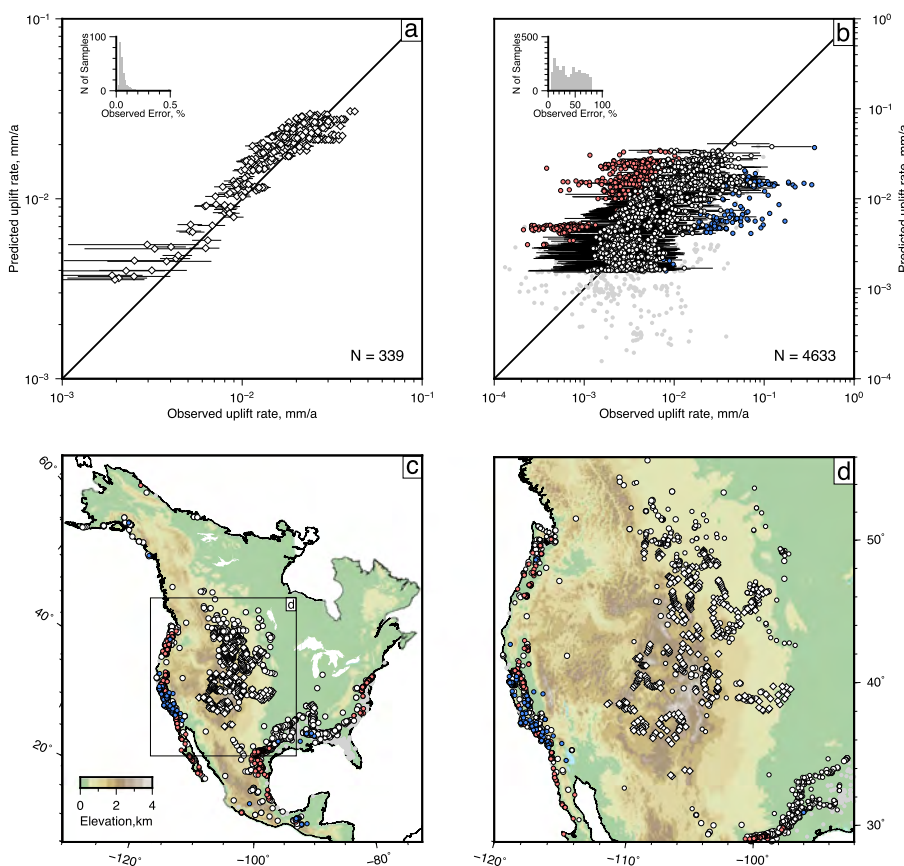


**Figure 9.** Testing results of inverse modeling. Comparison of time-averaged Late Cretaceous to Recent uplift from inverse model and (a) stratigraphic and (b) biostratigraphic constraints (Figures 4f–4n and 4a, respectively). Inset histograms = percentage error distribution of observations. Solid black line = 1:1 relationship; white circles = inverse results that agree with stratigraphic estimates; gray points = samples with large observational uncertainties (i.e., greater than 1 order of magnitude) with error bars omitted for clarity; red/blue points indicate where inverse model overpredicts/underpredicts uplift rate by more than a factor of 2. (c) Spatial distribution of stratigraphic and biostratigraphic constraints colored by accuracy of inverse model. Symbols same as for panels a and b. (d) Comparison of inverse modeling results and observations centered on Colorado Plateau (labeled box in panel c). Inverse model best matches uplift measurements across the Colorado Plateau and Rocky Mountains. Supporting information shows results obtained when erosional parameter,  $v$ , is increased/decreased by 1 order of magnitude.

Grande Embayment with fastest uplift rates between 20 and 10 Ma. Post-Cretaceous uplift of the Mexican Highlands generally exceeds 1 km. The southern and northernmost portions of these highlands were uplifted by almost 3 km and ~2 km, respectively. Along the eastern seaboard, our results suggest that the central Appalachian mountains were uplifted by ~1 km. The adjacent coastal plain underwent a maximum uplift of 300 m. Within cratonic North America, cumulative uplift is modest which suggests that the Canadian Shield and Interior lowlands have sat at relatively low elevation since Late Cretaceous times.

#### 4.5. Independent Tests

A significant advantage of an inverse modeling approach is that the predicted regional rock uplift as a function of space and time can be tested against independent observations. Here, we have carried out this testing by comparing predicted uplift histories with those determined from the biostratigraphic and stratigraphic inventory (Figure 4). The average uplift rate at each location was estimated from the age and elevation of the biostratigraphic sample. This value can be directly compared with the average predicted uplift rate, which is determined from the amount of cumulative uplift that has occurred since the time of deposition. We did not use samples that are younger than 5 Ma since the temporal resolution of the calculated uplift history is of O(5–10) Ma (Figure 8).

Comparison between observed stratigraphic and biostratigraphic constraints and predicted average uplift rate measurements are presented in Figure 9. Analysis of the smaller stratigraphic database shows that the inverse model yields a good agreement between observed and predicted uplift rates. Figure 9b presents a similar set of results for the much larger PBDB inventory. Open white circles comprise observations with relatively small uncertainties that are within an order of magnitude of the central value. In these cases, observed and predicted values agree to within a factor of 2. Gray circles also agree but have large observed uncertainties, principally because of relatively poorly constrained paleobathymetry. We conclude that calculated average uplift rates for most of the Colorado-Columbia-Rocky Mountains plateaus, the Appalachians, Texas, Mexican Highlands, Yukon, and the Great Plains are consistent with a combination of biostratigraphic and stratigraphic uplift measurements (Figures 9c and 9d).

There are two regions where the inverse model significantly overpredicts or underpredicts observed uplift rates: the Pacific Coastal Ranges and the Rio Grande Embayment. It is unsurprising that a damped inverse model yields a poorer fit along the Pacific Coast, which has experienced a complex tectonic history dominated by transcurrent plate motions and regional subsidence (e.g., Awater, 1970; Bartow, 1991). Overpredicted uplift rates within the Rio Grande Embayment are more problematic. The biostratigraphic compilation indicates that this embayment progressively shallowed from a deep marine Upper Cretaceous environment until Late Eocene times when deposits were predominantly deltaic or estuarine (e.g., Wilcox Formation; Galloway, 2001; Milliken et al., 2018). Since then, this region probably remained close to sea level, manifest by a record of Cenozoic shoreline progradation along the Coastal Plain (Galloway, 2001; Hosman, 1996). At present, the embayment is adjacent to the uplifted Sierra Madre province. Since relatively few rivers drain this region, there is lower model coverage, which is a possible reason why regional uplift has been overpredicted (Figures 1b and 8). We note that if the prefactor of the stream power relationship,  $v$ , is either decreased or increased by 1 order of magnitude, the resultant uplift history yields calculated rates that significantly mismatch stratigraphic and biostratigraphic constraints. These tests suggest that our calibrated value of  $v$  is a reasonable one (supporting information).

An assessment of model fidelity can also be made using additional independent uplift constraints (e.g., number of recorded extrusive events and clumped-isotope constraints). A two-stage Cenozoic uplift history of the Colorado Plateau is consistent with paleoaltimetric observations calculated from clumped isotopic analysis (Huntington et al., 2010). The distribution of extrusive magmatic events summarized in the NAVDAT database displays two broad peaks at  $\sim$ 80–55 Ma and at  $\sim$ 40–0 Ma (see, e.g., Chapin et al., 2004). In Alaska, three phases of magmatism centered at 33, 15, and 2 Ma have been recorded (Figure 2). Timing of peak magmatism is consistent with changes of predicted uplift rates (Figure 8b). In southern North America and Mexico, predicted regional uplift is consistent with the distribution of Cretaceous marine sedimentary rocks (Figure 4a; Bond, 1976; Sahagian, 1987). Along the Atlantic margin, Cretaceous marine sedimentary rocks also crop out, which is consistent with calculated regional uplift since the age of deposition. Between 30°N and 35°N, the elevation of an emergent Pliocene marine terrace increases from 20–30 to 60–80 m (Rowley et al., 2013). Calculated cumulative uplift in this region increases from  $\sim$ 40 Ma with higher rates between 30 Ma and the present day (Figure 8b).

The inverse model yields a good match to 100% and 86% of the stratigraphic and biostratigraphic inventories, respectively. We conclude that a continent-wide spatial and temporal uplift history calculated by inverting an inventory of 4,161 river profiles generally agrees with a suite of independent constraints. Our results build upon and are consistent with, nonlinear inverse modeling of a much smaller inventory of 93 river profiles (Roberts, White, et al., 2012).

## 5. Landscape Modeling

The inverse modeling procedure that we have described and applied can be further tested by landscape modeling. By forcing a landscape evolution model with the rock uplift rate history calculated by inverse modeling, testable predictions about elevation, drainage patterns, denudation, and sedimentary flux are made. In particular, the way in which the planform of drainage patterns evolves as it responds to regional uplift can be examined. In the future, it may prove possible to directly invert continental-scale topography for uplift and denudation using a landscape evolution model (e.g., Croissant & Braun, 2014). At present, guided forward

modeling is a pragmatic and computationally efficient approach for calculating continental-scale landscape evolution.

### 5.1. Badlands Algorithm

A modified version of the Basin and Landscape Dynamics (Badlands) model is used to calculate the spatial and temporal evolution of North American topography during the last 82 Ma together with discharge, denudation, and sedimentary flux (Salles, 2015). This landscape evolution model exploits a triangular mesh to solve the relevant geomorphic equations. Here, this mesh is generated from vertices with a regular spacing of 10×10 km. Drainage flow paths were determined using a single flow direction, steepest descent algorithm. Volumetric sedimentary flux was calculated across cell edges. The time steps are determined in accordance with a Courant-Friedrichs-Lowy condition to ensure numerical stability. As proposed by Salles (2015) a diffusion coefficient,  $\kappa=10^{-20}$  m<sup>2</sup>/Ma, is included to ensure model stability. We purposefully ensured that the forward model is kept as simple as possible and that the three erosional parameters,  $v$ ,  $m$ , and  $n$ , have identical values to those used for inverse modeling. Fixed Dirichlet boundary conditions were employed along the edges of the box to ensure that no interference with drainage development of the continental domain occurred. The model was not permitted to deposit sediment on the continent or along its margins, sea level was assumed to be constant, and precipitation rate,  $P$ , was set at unity. Finally, flexural responses to repartitioning of surface loads, glacial erosion, and ice cover were not included, and we made no corrections to the loci of paleoshorelines (cf. Salles et al., 2017; Wickert, 2016). The governing empirical equation takes the form

$$\frac{\partial z}{\partial t} = -v(AP)^m \nabla z - \kappa \nabla^2 z + U(x, y, t), \quad (8)$$

where  $U$  is the rock uplift rate history that was previously obtained by inverse modeling of the drainage inventory (Figure 8a). Incision rates (i.e.,  $\partial z / \partial t - U$ ) are easily extracted from numerical solutions of equation (8). In turn, these rates can be used to calculate cumulative denudation at spot locations by integrating incision rate with respect to time or to calculate sedimentary flux by integrating with respect to flow length in a downstream direction. We investigated the impact of four initial conditions on channelization and subsequent drainage planforms: a random distribution of slopes with small (i.e., meter-scale) relief, and 1%, 5%, and 10% of present-day topography (supporting information). These percentage fractions of present-day topography were calculated by multiplying the ASTER GDEM grid by 0.01, 0.05, and 0.1, respectively. By etching the initial condition (i.e., starting topography), the initial drainage pattern is set which subsequently evolves as the landscape develops. The impact of alternative uplift histories on calculated landscape evolution was investigated by rotating inserted rock uplift patterns by 90°. This test broadly preserves the amplitude-frequency content of inserted uplift (supporting information).

### 5.2. Calculated Landscape

Figure 10 presents elevation, discharge (i.e., drainage networks), cumulative denudation and sediment load as a function of geologic time for the last 70 Ma for a Badlands model that has a 5% initial condition. Unsurprisingly, this model predicts elevations at the present day that are similar to the ASTER GDEM topography (Figure 10a). In some locations, calculated elevations are lower than observed, especially within the Appalachian Highlands and Canadian Rockies, which we attribute to model smoothing. Calculated Cenozoic discharge suggests that the major continental-scale catchments (e.g., Mississippi, Colorado, Columbia, Yukon, and Mackenzie) are broadly stable. For example, most of the large rivers that drain western North America into the Gulf of Mexico have similar flow patterns over the last ~65 Ma, which is consistent with zircon provenance measurements from Cretaceous and Paleocene fluvial sandstones along the northern margin of the Gulf of Mexico (Figure 2; Blum & Pecha, 2014; Blum et al., 2017). Similar results have been obtained for the random slope condition and for the 1% initial condition. Drainage planforms are more entrenched for the 10% initial condition (supporting information). One concern is that the cell size used to parameterize the landscape evolution model can potentially force the drainage planform to remain fixed (Goren et al., 2014). This concern was examined by changing the inserted rock uplift history. In these tests, the initial condition (5% of present-day topography) was kept the same as for the earlier test. Results show that calculated planforms (e.g., rivers and drainage divides) do indeed adjust and change as the landscape develops, in accordance with the pattern of forcing uplift.

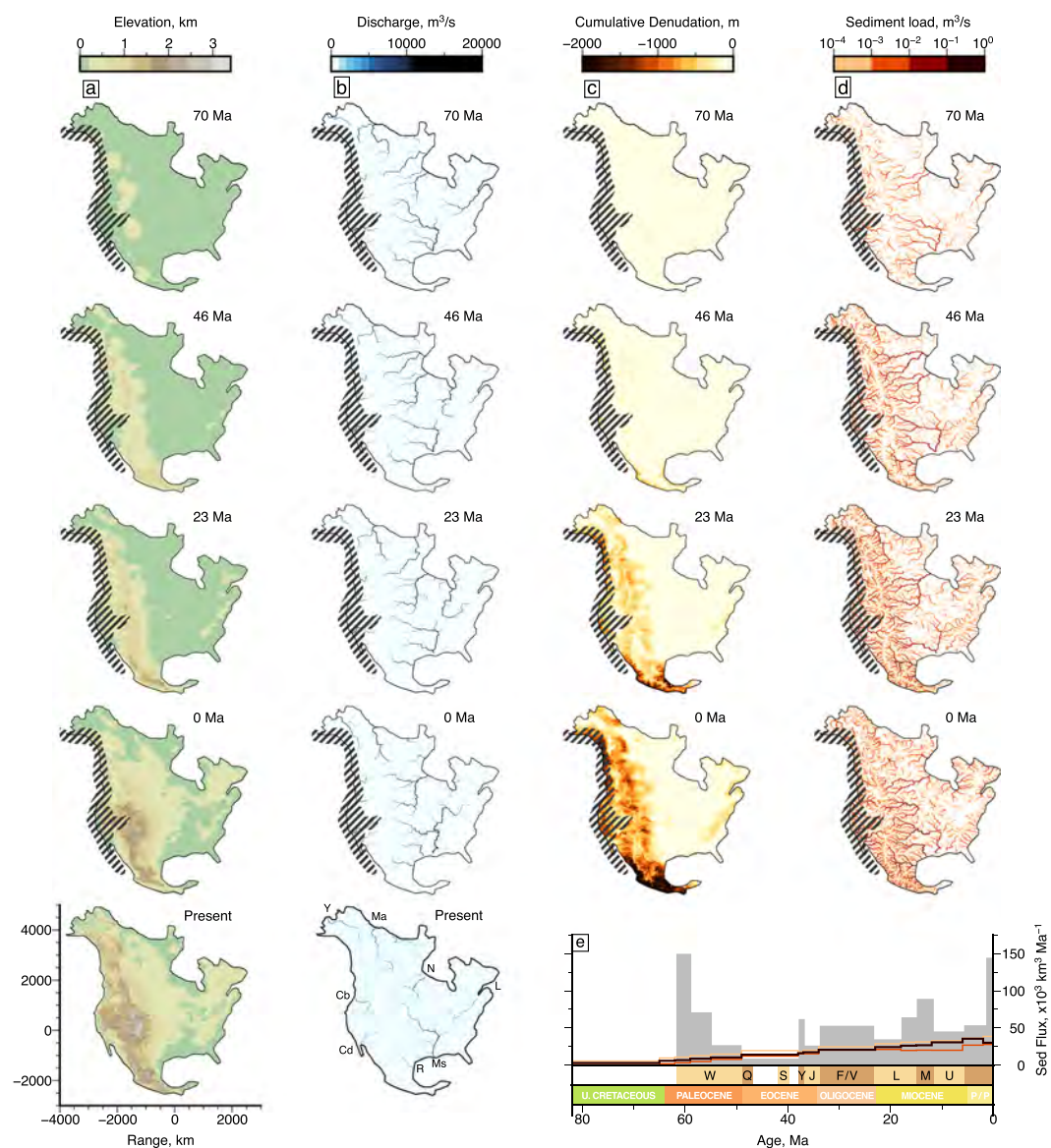


**Figure 10.** Predicted landscape evolution. (a) Late Mesozoic and Cenozoic topographic evolution of North America calculated using modified version of Badlands landscape evolution model (Salles, 2015). Model was forced using uplift history calculated by inverse modeling (Figure 8). Model resolution = 10 km. Hatched region = portion of model where calculated uplift history should be treated with caution. Lowest panel = present-day topography from ASTER GDEM database for comparison. (b) Calculated discharge. Bottom panel = present-day discharge calculated using Esri flow-routing algorithms and ASTER GDEM database (see Figure 1 for annotation). (c) Calculated cumulative denudation (i.e.,  $\int \partial z / \partial t$ ). (d) Calculated sedimentary load (i.e.,  $\int \partial z dx / \partial t$ ). (e) Gray histogram = observed solid sedimentary flux for Gulf of Mexico redrawn from Galloway et al. (2011). Orange/black/red lines = flux calculated for three different Badlands landscape evolution models parameterized using 1%, 5%, and 10% starting conditions (see supporting information). Brown/peach band shows stratigraphy: W = Wilcox; Q = Queen City; S = Sparta; Y = Yegua; J = Jackson; F/V = Frio/Vicksburg; L, M, U = Lower, Middle, and Upper Miocene. Note model coverage is <20% before 55 Ma (see Figure 7c). ASTER = Advanced Space-borne Thermal Emission and Reflection Radiometer; GDEM = global digital elevation model.

### 5.3. Denudational History

Thermochronometric measurements provide an additional means of estimating denudation over long time scales. In essence, these techniques record the temperature of rocks as a function of time. By relating these histories to estimates of crustal temperatures, it is possible to extract denudational histories (see, e.g., Farley, 2002; Gallagher, 1995; Gleadow & Brown, 1999; Green et al., 1989). A key result from thermochronometers

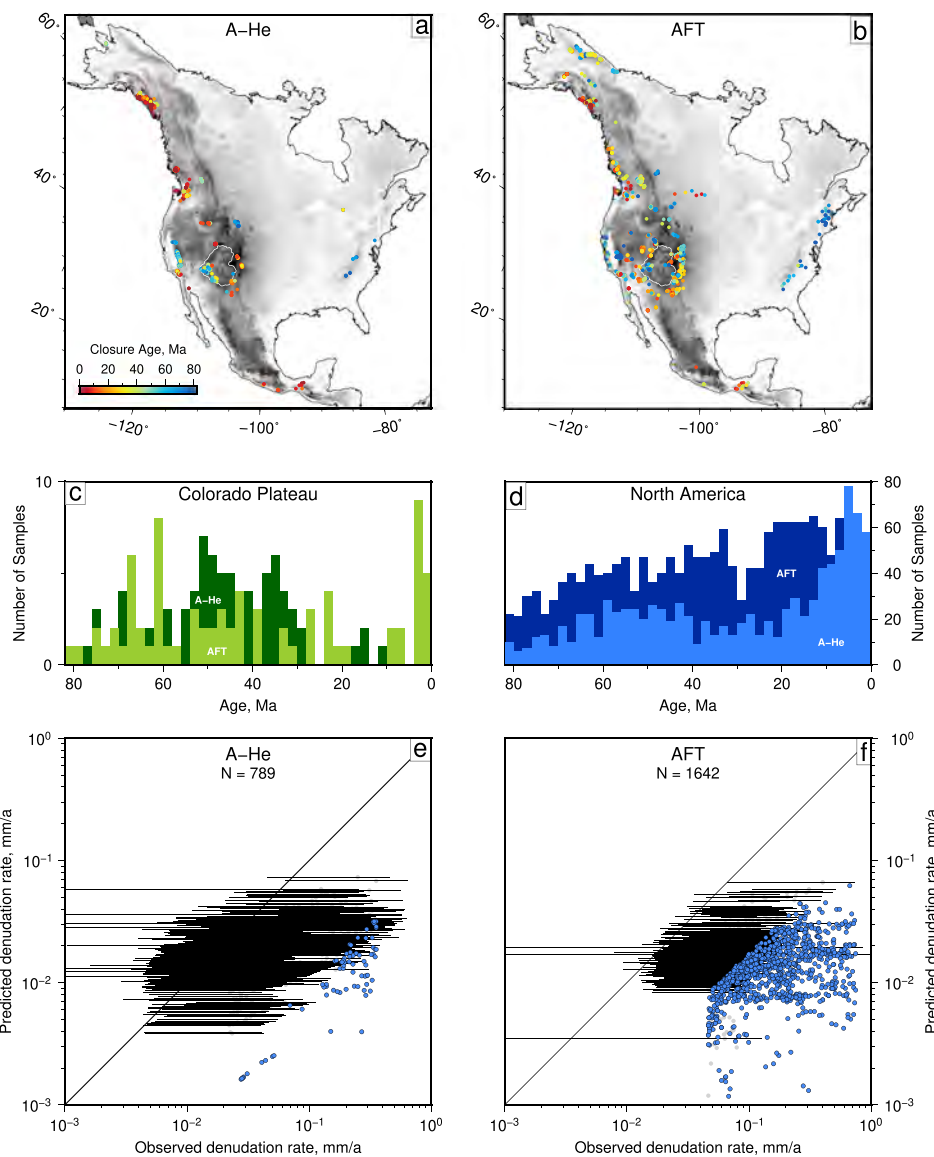


**Figure 11.** Comparison of thermochronometric and calculated denudation rates. (a) Synthesis of independent estimates of U-Th/He (A-He) closure ages for North America. Gray shading = present-day topography calculated from ETOPO1 database; thin white line encloses Colorado Plateau. (b) Apatite fission track (AFT) closure ages. (c) Histograms of A-He and AFT closure ages from Colorado Plateau. (d) Histograms of closure ages for North America. (e) Comparison of denudation rates calculated from landscape evolution model that was parameterized using results of inverse modeling (Figure 10c) and independent A-He closure ages (see panels a and b). Error bars = data where match between the parameterized forward model and independent estimates is good; blue points = data where calculated denudation rates are factor of 2 or more lower than A-He estimates where error bars have been omitted for clarity (see supporting information). (f) Comparison of calculated denudation rates and independent estimates from AFT closure ages.

is the age at which rock has cooled below the closure temperature of the individual system. The presence of cooled rock at Earth's surface today is usually interpreted as removal of overburden by denudation. We have tested our predicted denudation history by exploiting the results from two well-known low-temperature thermochronometers: AFT and apatite (U-Th)/He (A-He). Our principal aim is to investigate how well the landscape evolution model, which was parameterized using a smoothly varying rock uplift history, can reproduce independent estimates of exhumation. Our compilation of thermochronometric results builds on previous inventories and includes 1,642 AFT and 789 A-He closure ages from North America (e.g., Herman et al., 2013; Slone et al., 2003; U.S. Geological Survey National Geochronology Database;

supporting information). The spatial and temporal distribution of this compilation is presented in Figures 11a–11d. We have attempted to identify samples with cooling histories that have been overprinted by tectonic and/or magmatic events and manually excised them from the compilation.

Figure 11d shows there are three broad peaks evident within AFT closure age measurements: 80–60, 50–30, and 30–10 Ma. The number of measurements of A-He closure ages is greatest between ~20 Ma and the present day. Thermobarometric modeling and rock cooling histories suggest that Cenozoic denudation rates across southern North America and Mexico were highest during the last 40 Ma (Gray et al., 2001; Montgomery & López-Blanco, 2003; Ferrari et al., 2012). One interpretation of this trimodal distribution is that North America has experienced at least three discrete kilometer-scale phases of Late Mesozoic to Recent denudation. However, we acknowledge that this database has significant spatial bias; coverage is greatest on the Colorado-Columbia-Rocky Mountains plateaus, along parts of the Appalachian mountains, Mexican highlands, and within the Yukon region (Figures 11a and 11b). Portions of the Colorado Plateau that have a two-stage Cenozoic cooling history have been interpreted as evidence for an ancestral Colorado River. We note that alternative explanations exist (see, e.g., Flowers & Farley, 2012; Karlstrom et al., 2014). Late Cretaceous to Early Paleocene A-He and AFT ages along the Appalachian mountains suggest that ~2 km of overburden has been removed during the last ~60 Ma. Closure ages along the northern Pacific Coastal Ranges are mostly younger than 50 Ma. In the north and central Rocky Mountains, closure ages are between 70 and 40 Ma, which is broadly coeval with the timing of Laramide tectonism (e.g., Dickinson et al., 1988; Peyton & Carrapa, 2013). In the Southern Rockies and Rio Grande Rift, there are a suite of A-He and AFT closure ages <40 Ma. Kelley and Chapin (1995) and Peyton and Carrapa (2013) related this post-Laramide cooling to burial, subsequent epeirogenic uplift and removal of sedimentary rocks while the Rio Grande Rift developed. O'Sullivan and Currie (1996) and O'Sullivan and Lane (1997) propose that the Yukon plateau has had a staged denudation history, with cooling phases between 60 and 40 Ma, and at ~15 Ma.

In order to compare this compilation with our predictions, we first convert reported closure ages into average denudation rates. Temperature histories of rocks can be extracted by inverting apparent ages and fission track length distributions (Ketcham, 2005; Gallagher, 2012). However, it is still unclear how spatial averaging of cooling histories, rates of exhumation at the time of closure, and time-dependent geothermal gradients affect these results (Schildgen et al., 2018). Here, we use a simple expression that relates surface and closure temperatures,  $T_s$  and  $T_c$ , geothermal gradient,  $dT/dz$ , and closure age,  $a_c$ , in order to calculate the time-averaged denudation rate, which is given by

$$\frac{dz}{dt} = \frac{T}{a_c(dT/dz)}, \quad (9)$$

where  $T=T_c-T_s$ . Measurement errors and uncertainties in the thermal properties of the crust were propagated to obtain

$$\delta_{dz/dt} = \left| \frac{dz}{dt} \right| \sqrt{\left( \frac{\delta_T}{|T|} \right)^2 + \left( \frac{\delta_{dT/dz}}{|dT/dz|} \right)^2 + \left( \frac{\delta_{a_c}}{|a_c|} \right)^2}, \quad \delta_T = \sqrt{(\delta_{T_c})^2 + (\delta_{T_s})^2}. \quad (10)$$

These errors can also be gauged by using extremal values of the variables. Significant uncertainties include closure temperatures, which vary between  $110 \pm 10$  °C for AFT and  $\sim 60 \pm 30$  °C for A-He, although a larger range for AFT is sometimes reported (Dodson, 1973; Green et al., 1989; Reiners & Brandon, 2006). Geothermal gradients can be affected by changes in basal heat flow, by the distribution of radiogenic elements, and by thermal advection. We tested a suitable range of geothermal gradients ( $25 \pm 15$  °C/km), which broadly encompasses those values reported for radiogenic to weakly radiogenic crust. These values are the most significant control for crustal temperatures of unstretched lithosphere (e.g., McKenzie et al., 2005). Surface temperatures are often poorly constrained, and we assumed that  $T_s=15 \pm 10$  °C (see, e.g., Greenwood & Wing, 1995). We acknowledge that more complex thermokinetic models exist, which incorporate, for example, the effects of two- and three-dimensional conductive cooling and advection of heat (e.g., Braun, 2002). In our view, the uncertainties in thermal structure of the crust and its time-dependent

behavior mean that simple models are justifiable in this instance. For each sample, denudation rate and associated error were calculated using equations (9) and (10) (supporting information).

It is important to emphasize that rock uplift without concomitant denudation is difficult to detect using thermochronometric techniques. Conversely, rapid erosion can in principle produce significant denudation in the absence of surface uplift. One way to examine the cause of rock cooling and its relationship with uplift is to extract denudational estimates from parametrized landscape evolution models. Here, we use the compilation of rock cooling rates to test predicted values (Figure 10). It is important that these rates are compared at the same location and for the timescale determined by the closure age of the thermochronometric measurement. We avoided comparing samples with closure ages younger than 6 Ma, which is the limit of resolution for our landscape model. Furthermore, young AFT (or AHe) ages that are <5 Ma can be affected by thermal advection which we have ignored for simplicity (Lisker et al., 2009). A comparison between observed and predicted denudation rates is presented in Figures 11e and 11f. For clarity, uncertainties are shown for samples where our model matches thermochronometric measurements within error (plus or minus a factor of 2), representing 90% of the A-He and 36% AFT samples in our inventory. Samples where denudation cannot be predicted within error are shown as blue circles. The landscape evolution model underpredicts 10% and 64% of the A-He and AFT measurements, respectively. One way to interpret these results is that A-He closure ages are more closely related to the formation of the modern landscape than AFT measurements. Rock cooling histories can be sensitive to short wavelength tectonic processes and abrupt changes of denudation rate are unlikely to be expressed in the smooth landscape evolution model presented here. Finally, fission track annealing can result in bias toward younger AFT ages, and therefore higher denudation rates, which is consistent with systematic underprediction.

## 6. Discussion

### 6.1. Continental Epeirogeny

The stratigraphic and biostratigraphic inventories that we exploit were taken from a substantial body of published paleoaltimetric constraints. They provide excellent evidence for staged regional Cenozoic growth of North American topography, with at least 2 km of topography having been generated since Campanian times (~82 Ma; Figure 2; Chamberlain et al., 2012). To further explore and constrain the history of vertical motions and subplate support, we solved for spatially and temporally smooth rock uplift histories by inverting a continental inventory of river profiles. This inverse model was calibrated using a small number of incision rates from the Colorado Plateau (Karlstrom et al., 2008; Roberts, White, et al., 2012). The calculated uplift history is consistent with the independent inventory of stratigraphic and biostratigraphic uplift constraints across the Colorado-Columbia-Rocky Mountains plateaus, for large portions of the Appalachian Mountains, for Mexico and for the Gulf Coast. It is also broadly consistent with a range of other independent uplift constraints (e.g., clumped and stable isotopes and magmatism; Chamberlain et al., 2012; Fitton et al., 1991; Huntington et al., 2010). Calculated uplift from the Rockies to Great Plains suggests that regional tilting developed during the last ~10 Ma, which is consistent with tilting histories recorded by the Late Miocene Ogallala Group and by the Pliocene Broadwater Formation adjacent to the North Platte river (Duller et al., 2012; Willett et al., 2018). The model performs poorly where there has been significant lateral tectonic displacements (e.g., Pacific seaboard) or where spatially smooth uplift histories are less appropriate. Despite the simplicity of the inverse modeling scheme, there is a reasonable match between timing of uplift and location of paleoshorelines inferred from the biostratigraphic inventory and from previous studies (Figure 12; Kauffman & Caldwell, 1993; Roberts & Kirschbaum, 1995; Smith et al., 1994; Ziegler et al., 1985).

Observed and calculated uplift rates are broadly consistent and suggest that North American topography grew in several stages. These results imply that drainage planforms tend to respond to changes in uplift rate in a predictable fashion, which can be exploited to investigate continental-scale histories of regional uplift. An important test of this approach is to compare calculated uplift and denudation with independent observations. In Figures 9 and 11, we show that a simple erosional model can yield results that provide a reasonably good match. The calibrated value of  $v$  is appropriate for extracting continental-scale uplift histories from drainage (supporting information). These combined results provide additional constraints for the driving mechanisms of continental epeirogeny (Figure 12).

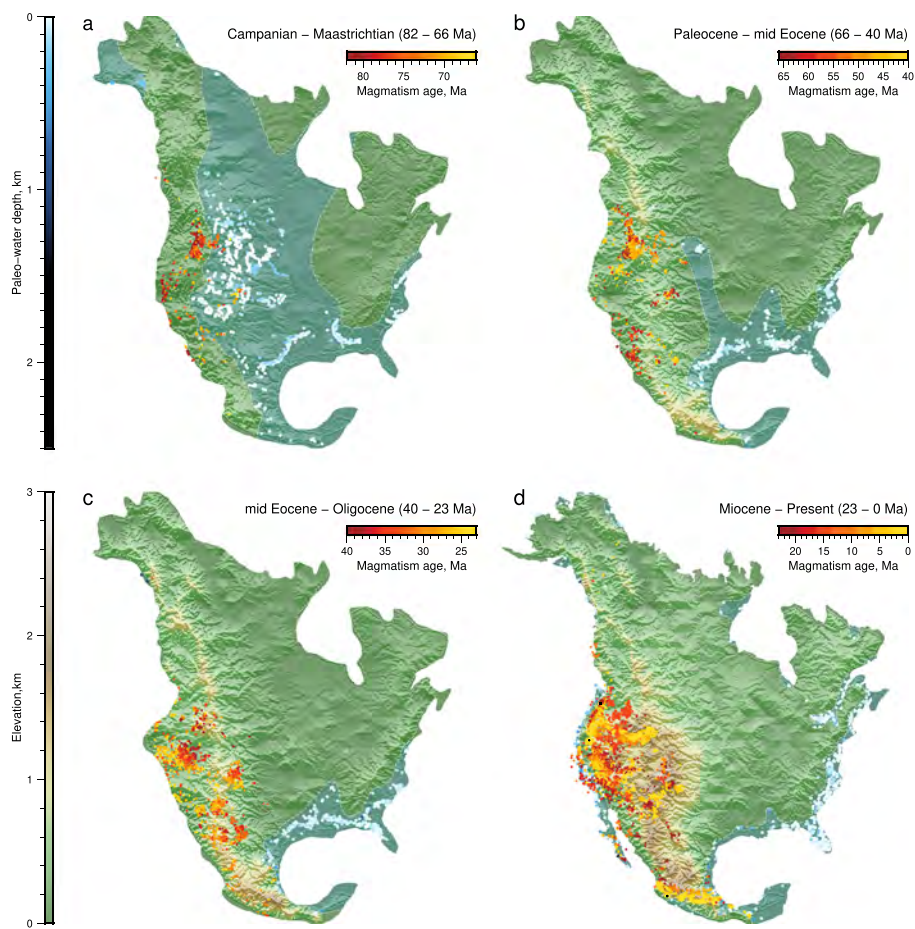


**Figure 12.** Landscape evolution model of North America. (a–d) Four panels show calculated Mesozoic to Cenozoic topographic evolution compared with coeval independent paleogeographic constraints. Red circles = magmatic record from NAVDAT database (Figure 2); blue circles = stratigraphic shoreline markers/marine fossils from PBDB (Figure 4); light blue shading = maximum flooded surface from Smith et al. (1994) revised with stratigraphic and biostratigraphic constraints presented here.

## 6.2. Consequences for Landscape Evolution

The inverse modeling strategy that we have described and applied makes a series of simplifying assumptions that warrant further discussion. With regard to the drainage evolution of North America, there are three significant concerns: simplicity of our erosional model, stability of the drainage planform, and the influence of glaciation.

First, we have assumed a simplified version of the nonlinear stream power erosional model. This model appears to be sufficiently complex to fit large inventories of river profiles with geologically meaningful uplift rate histories in that they are comparable to independent constraints (e.g., Figure 9). This model assumes that the values of the erosional parameters,  $v$  and  $m$ , are constant and that shock waves are unimportant at long wavelengths (i.e.,  $n=1$ ; equations (2) and (8)). Implicit in these assumptions is that substrate (e.g., bedrock lithology and alluvium), biota, hydrodynamic processes, and changes in climate (e.g., precipitation and discharge) do not set the pace of landscape evolution at long wavelengths and timescales of tens of millions of years. More generally, poor correlations between substrate (or change in substrate) as a function of river elevation, slope, curvature, or calculated stream power at wavelengths greater than a few kilometers support the suggestion that lithology may not control channel geometry at wavelengths of more than a few kilometers (Czarnota et al., 2014; Paul et al., 2014; Roberts, White, et al., 2012). These observations are consistent with spectral analyses of longitudinal river profiles, which indicate that their shapes are dominated by wavelengths  $>10$  km and that river profiles from adjacent catchments contain commonalities

generated by regional uplift (Roberts et al., 2019; Roberts, 2019). Nevertheless, there is a substantial body of work which demonstrates that at smaller scales these processes determine the efficacy of fluvial erosion and the geometry of river profiles (e.g. Armitage et al., 2018; Baynes et al., 2018; Forte & Whipple, 2018; Gallen, 2018). It is unclear how these complex, dynamic, threshold-dependent, and undoubtedly nonlinear, processes scale over geologic timescales. However, at a continental scale, we propose that the long-wavelength portions of landscapes are controlled by regional uplift but moderated by integrated fluvial erosion through time and space in a predictable way.

The way in which erosion scales with slope is debated. For example, the value of the slope exponent in the stream power model,  $n$ , might range between 2/3 to 5/3 or greater, and may be location, process and scale dependent (e.g., Attal et al., 2008; Howard & Kerby, 1983; Lague, 2014; Whipple & Tucker, 1999; Whittaker & Boulton, 2012). If  $n>1$ , then information about tectonic history may be lost from longitudinal river profiles (e.g., Pritchard et al., 2009; Royden & Perron, 2013). However, several observations exist that suggest that the integrated history of fluvial erosion on scales of  $O(10^2\text{--}10^3)$  km and  $O(1\text{--}10)$  Ma may depend linearly on slope. For instance, (Czarnota et al., 2014) shows that there is a global minimum at  $n=1$  by minimizing misfit between modeled and observed longitudinal river profiles of modern and ancient thalwegs of the Tumut river, Eastern Australia. In general, testing and validation of fluvial erosional models at long wavelengths and timescales is difficult (Salles et al., 2017). Large inventories of independent constraints on surface and rock uplift can be used to evaluate the success of erosional models (see supporting information). The simple, linear version of the stream power erosion model we use appears to provide sufficient complexity to match observed longitudinal river profiles and reproduce meaningful uplift histories. However, we acknowledge that at short timescales and length scales, more complex erosional models might be more appropriate.

A second and related issue concerns the evolution of drainage planforms (e.g., Willett et al., 2014). There is much uncertainty about the longevity of drainage networks. Changing drainage planforms by divide migration or by stream capture should, with time, rearrange catchment planforms thus rendering attempts to extract information about uplift signal problematic, especially over long temporal and spatial scales. However, a small number of observations suggest that, at large scales, the assumption of essentially fixed drainage planforms could be a reasonable one. First, laboratory sandbox experiments point to the importance of preexisting topography in determining the fixity of drainage divides and the extent to which they can migrate under changing experimental conditions (e.g., Bonnet, 2009; Lague et al., 2003). We note that fluvial systems have been used to infer lateral migration of drainage divides by using simple geomorphic parameters (e.g.,  $\chi$ ). Unfortunately, use of these simple metric values require unreasonable assumptions about the spatial pattern of uplift rate which are demonstrably incorrect, especially at continental length scales (Herman & Braun, 2006).

Landscape evolution models suggest that drainage divide migration is not especially significant and in any case the inverse modeling presented here is robust to large excursions in values of upstream drainage area since  $A$  is taken to a fractional power. Nonetheless, we can examine how calculated uplift histories are affected by changing drainage planform by comparing our results with the history of long-term planform evolution inferred by detrital zircon studies (Blum & Pecha, 2014). In Figure 2, we summarize measurements of detrital zircon ages along the northern margin of the Gulf of Mexico. Figure 2e shows crustal and magmatic zircon source terranes adapted from Figure DR5 of Blum and Pecha (2014) where the cumulative percentage plots of Figure 2f were redrafted from their Figure DR6. Their observations suggest that the Paleocene drainage planform had a broadly similar distribution to that of the present day. For example, >50% of the zircons in Paleocene samples close to the eastern tributaries were derived from the Grenville (1250–950 Ma), Mid-Continent (1500–1300 Ma), and Appalachian (750–280 Ma) terranes (e.g., sample 43). Paleocene samples located west of the Mississippi River have >50% of zircons ages that correspond to the Yavapai-Mazatzal (1800–1600 Ma) and Western Cordillera (275–50 Ma) terranes (e.g., sample 64). These observations imply the large-scale planform of the Mississippi catchment may not have significantly changed during Cenozoic times.

Another way to estimate longevity of drainage patterns is to compare observed and predicted sedimentary flux. Sedimentary flux was calculated by integrating incision rate in a downstream direction using the landscape evolution model shown in Figure 10. The tectonic history of western North America complicates

interpretation of sedimentary flux observations from, for example, the Los Angeles basin or Baja California (see, e.g., Dorsey et al., 2018). In contrast, the Gulf of Mexico appears to have acted as a stable depositional sink since Cretaceous times (Galloway et al., 2000). Figures 10c–10e compare predicted to independent estimates of flux in the Gulf of Mexico (Galloway et al., 2011). Calculated cumulative denudation is highest in the regions of highest predicted uplift rates (e.g., Rocky Mountains–Colorado plateaus, Appalachian Mountains, Yukon, and Mexican Highlands). Predicted sedimentary flux is smoother than that measured by Galloway et al. (2011), which is unsurprising because the landscape model was parameterized using a damped, smooth, rock uplift history. The biggest discrepancy between predicted and observed flux is at ~60 Ma (e.g., the Wilcox Formation). We note that model coverage in the headwaters of the Mississippi catchment is low before ~55 Ma (Figure 10c).

Finally, we have ignored the possible effects of glacial erosion and widespread continental ice cover during the last glacial maximum, partly for simplicity but mostly because it is not obvious how this issue can be addressed in a transparent way. Most of the area that was covered by ice sheets is located within the cratonic regions of northern and eastern Canada where glacial isostatic rebound continues to be the driver of surface uplift. Temporal resolution of the inverse model presented here is too coarse to accurately compute the effect of this glacial signal. The effect that extensive ice sheets could have upon drainage planform and their efficiency in topographic erosion relative to fluvial processes are poorly understood. For example, global compilations of erosion rates from glaciers and rivers on timescales of  $10^1$ – $10^7$  years implies that glacial erosion tends to decrease by 1 to 2 orders of magnitude over glacial cycles, whereas fluvial erosion rates reveal no such dependence upon time. This observation suggests that uplift histories control rates of both fluvial and glacial erosion over millennial and longer timescales (Koppes & Montgomery, 2009). It remains unclear how drainage planforms were dramatically modified by the last glacial maximum (~21 ka; Wickert, 2016). Geologic constraints for the uplift and denudation history of a region covered by the Laurentide ice sheet are sparse (Figures 2 and 4). Additional testing of the results of our inverse model for this region would be insightful.

### 6.3. Geodynamic Implications

Both orogenic and epeirogenic processes can generate topography. Shortening, extension, magmatic underplating, and dynamic uplift all contribute toward continental uplift, and, to some extent, these phenomena can be discriminated based upon their magnitude and wavelength (e.g., Pazzaglia & Brandon, 1996). Cretaceous uplift of the Rocky Mountains region was partially caused by growth of Laramide-aged structures (Figures 4 and 5). The geomorphic modeling and stratigraphic observations presented here suggest that regional uplift of western North American topography has predominated. Isostatic considerations indicate that the present-day surface elevation of this extensive region is supported by density variations within and beneath the lithospheric mantle rather than by crustal thickening (e.g., Levandowski et al., 2018). Rare earth element inverse modeling of <5 Ma basaltic melts with Ocean Island Basalt affinities combined with the presence of shear wave velocity anomalies constrained by earthquake tomographic models are consistent with moderately elevated mantle potential temperatures and thin (~70 km) lithosphere beneath western North America (Klocking et al., 2018). These observations support the notion that large-scale dynamic topography is generated and maintained by temperature anomalies within asthenospheric mantle directly beneath a thin plate. The detailed driving mechanisms that underpin observed and predicted vertical displacements have been explored by a range of numerical flow models on different temporal and spatial scales (see, e.g., Forte et al., 2009; Lithgow-Bertelloni & Gurnis, 1997; Liu et al., 2008; Liu, 2014; Mitrovica et al., 1989; Moucha et al., 2016; Rowley et al., 2013; Spasojević et al., 2009; Spasojević & Gurnis, 2012; van Wijk et al., 2010). The results from this study could provide additional constraints for such models.

## 7. Conclusions

Cenozoic evolution of the North American landscape is determined by combining constraints provided by stratigraphic and biostratigraphic databases with inverse and forward modeling of drainage inventories. Average uplift rates estimated from fossil and stratigraphic data suggest that, following the retreat of the Western Interior Seaway at ~80 Ma, western North America experienced staged uplift of up to 3 km. The Yukon, Appalachian Mountains, and Mexico mostly underwent Neogene uplift. By inverting 4,161

longitudinal river profiles, assuming a simplified version of the widely used stream power relationship, we have generated a smooth spatiotemporal uplift history that fills the gaps between spot stratigraphic and biostratigraphic constraints. Mapped drainage planforms indicate that North American rivers flow radially from large-scale swells, which have wavelengths of the order 100–1,000 km. The principal swells are centered on the Colorado-Columbia-Rocky Mountains plateaus, Yukon, Appalachians, and Mexico where subplate dynamic support is important. Predicted regional uplift rates of the Colorado-Columbia-Rocky Mountains plateaus increased from ~0.02 mm/a between 80 and 50 Ma to ~0.1 mm/a between 30 and the present day. To estimate denudation and to examine sensitivities of drainage patterns to tectonic forcing, we parameterized the Badlands landscape evolution model using the inverted uplift history. The results of this forward simulation is compared with a synthesis of independent estimates of denudation from thermochronometric studies and with continent-wide provenance analyses.

Several significant implications are apparent. First, substantial compilations of stratigraphic observations can be used to gauge uplift and denudation rates at large length and timescales. Second, drainage patterns can be inverted by assuming a simplified version of the stream power relationship despite the apparent complexity of eroding landscapes. This modeling approach provides a useful way to constrain uplift histories on continental scales. Finally, measured and calculated uplift and denudation histories are consistent with Cenozoic sub-plate support which seems to have played a defining role in generating the North American landscape, especially at wavelengths greater than a few tens of kilometers.

#### Acknowledgments

We thank E. Kite, C. O'Malley, P. Mannion, C. Pont, C. Richardson, D. Rowley, J. Rudge, S. Stephenson, and A. Wickert for helpful discussion. We are grateful to S. Willett for providing a helpful and insightful review. sf NAVDAT database can be accessed online ([www.navdat.org](http://www.navdat.org)), sf ASTER GDEM data can be downloaded online (<http://gdem.ersdac.jspacesystems.or.jp>), sf SRTM database can be downloaded online ([srtm.csi.cgiar.org](http://srtm.csi.cgiar.org)), and Paleobiological database can be accessed online (<https://paleobiodb.org/>). sf PaleoDB data were downloaded on 25 October 2017 for Campanian, Maastrichtian, and Cenozoic time intervals. Cambridge Earth Sciences Contribution esc.4514.

#### References

- Ainsworth, N. R., Riley, H., Bailey, W., & Gueinn, K. J. (2014). Cretaceous–Tertiary stratigraphy of the Labrador Shelf, Riley Geoscience Ltd.commissioned by Nalcor Energy, <http://www.nalcorenergy.com/OILGAS/labrador-biostratigraphy.asp>
- Allen, G. H., Barnes, J. B., Pavelsky, T. M., & Kirby, E. (2013). Lithologic and tectonic controls on bedrock channel form at the northwest Himalayan front. *Journal of Geophysical Research: Earth Surface*, 118, 1806–1825. <https://doi.org/10.1002/jgrf.20113>
- Amidon, W. H., Roden-Tice, M., Anderson, A. J., McKeon, R. E., & Shuster, D. L. (2016). Late Cretaceous unroofing of the White Mountains, New Hampshire, USA: An episode of passive margin rejuvenation? *Geology*, 44(6), 415–418. <https://doi.org/10.1130/G37429.1>
- Anderson, R. S., & Anderson, S. P. (2010). *Geomorphology: The mechanics and chemistry of landscapes*. United Kingdom: Cambridge University Press.
- Armitage, J. J., & Allen, P. A. (2010). Cratonic basins and the long-term subsidence history of continental interiors. *Journal of the Geological Society of London*, 167(1), 61–70. <https://doi.org/10.1144/0016-76492009-108>
- Armitage, J. J., Whittaker, A. C., Zakari, M., & Campforts, B. (2018). Numerical modelling of landscape and sediment flux response to precipitation rate change. *Earth Surface Dynamics*, 6, 77–99.
- Arthur, M. A., & Sageman, B. B. (2004). Sea-level control on source-rock development: Perspectives from the Holocene Black Sea, the Mid-Cretaceous Western Interior Basin of North America, and the Late Devonian Appalachian Basin. *SEPM Special Publication*, 82, 35–59.
- Attal, M., Tucker, G. E., Whittaker, A. C., Cowie, P. A., & Roberts, G. P. (2008). Modelling fluvial incision and transient landscape evolution: Influence of dynamic channel adjustment. *Journal of Geophysical Research*, 113, F03013. <https://doi.org/10.1029/2007jf000893>
- Ault, A. K., Flowers, R. M., & Bowring, S. A. (2013). Phanerozoic surface history of the Slave craton. *Tectonics*, 32, 1066–1083. <https://doi.org/10.1002/tect.20069>
- Awatere, T. (1970). Implications of plate tectonics for the Cenozoic tectonic evolution of Western North America. *Geological Society of America Bulletin*, 81, 3513–3536.
- Baldwin, J. A., Whipple, K. X., & Tucker, G. E. (2003). Implications of the shear stress river incision model for the timescale of postorogenic decay of topography. *Journal of Geophysical Research*, 108(B3), 2158. <https://doi.org/10.1029/2001JB000550>
- Bartow, J. A. (1991). Cenozoic evolution of the San Joaquin Valley, California. *United States Geological Survey Professional Paper*, 1501, 1–40.
- Baynes, E., Lague, D., Attal, M., Gangloff, A., Kirstein, L. A., & Dugmore, A. J. (2018). River self-organisation inhibits discharge control on waterfall migration. *Science Reporter*, 8, 1–8. <https://doi.org/10.1038/s41598-018-20767-6>
- Becker, T. W., Faccenna, C., Humphreys, E. D., Lowry, A. R., & Miller, M. S. (2014). Static and dynamic support of western United States topography. *Earth and Planetary Science Letters*, 402(C), 234–246. <https://doi.org/10.1016/j.epsl.2013.10.012>
- Best, M. G., Barr, D. L., Christiansen, E. H., Gromme, S., Deino, A. L., & Tingey, D. G. (2009). The Great Basin Altiplano during the middle Cenozoic ignimbrite flareup: Insights from volcanic rocks. *International Geology Review*, 51(7–8), 589–633. <https://doi.org/10.1080/00206810902867690>
- Blum, M. D., Milliken, K. T., Pecha, M. A., Snedden, J. W., Frederick, B. C., & Galloway, W. E. (2017). Detrital-zircon records of Cenomanian, Paleocene, and Oligocene Gulf of Mexico drainage integration and sediment routing: Implications for scales of basin-floor fans. *Geosphere*, 13(6), 2169–2205. <https://doi.org/10.1130/GES01410.1>
- Blum, M., & Pecha, M. (2014). Mid-Cretaceous to Paleocene North American drainage reorganization from detrital zircons. *Geology*, 42(7), 607–610. <https://doi.org/10.1130/G35513.1>
- Boettcher, S. S., & Milliken, K. L. (1994). Mesozoic-Cenozoic unroofing of the Southern Appalachian Basin: Apatite fission track evidence from Middle Pennsylvanian sandstones. *Journal of Geosciences*, 102(6), 655–668. <https://doi.org/10.1086/629710>
- Bond, G. (1976). Evidence for continental subsidence in North America during the Late Cretaceous global submergence. *Geology*, 4, 557–560.
- Bonnet, S. (2009). Shrinking and splitting of drainage basins in orogenic landscapes from the migration of the main drainage divide. *Nature Geoscience*, 2(11), 766–771. <https://doi.org/10.1038/ngeo666>

- Braun, J. (2002). Quantifying the effect of recent relief changes on age-elevation relationships. *Earth and Planetary Science Letters*, 200, 331–343.
- Brocard, G. Y., & Van Der Beek, P. (2006). Influence of incision rate, rock strength, and bedload supply on bedrock river gradients and valley-flat widths: Field-based evidence and calibrations from western Alpine rivers (southeast France). *Geological Society of America Special Papers*, 398(07), 101–126. [https://doi.org/10.1130/2006.2398\(07\)101-126](https://doi.org/10.1130/2006.2398(07)101-126)
- Brocard, G. Y., Willenbring, J. K., Miller, T. E., & Scatena, F. N. (2016). Relict landscape resistance to dissection by upstream migrating knickpoints. *Journal of Geophysical Research: Earth Surface*, 121, 1182–1203. <https://doi.org/10.1002/2015JF003678>
- Bustin, R. M. (1991). Organic maturity in the western Canada sedimentary basin. *International Journal of Coal Geology*, 19, 319–358.
- Campforts, B., & Grovers, G. (2015). Keeping the edge: A numerical method that avoids knickpoint smearing when solving the stream power law. *Journal of Geophysical Research: Earth Surface*, 120, 1189–1205. <https://doi.org/10.1002/2015JF003600>
- Cao, W., Zahirovic, S., Flament, N., Williams, S., Golonka, J., & Dietmar Müller, R. (2017). Improving global paleogeography since the late Paleozoic using paleobiology. *Biogeosciences*, 14(23), 5425–5439. <https://doi.org/10.5194/bg-14-5425-2017>
- Cassel, E. J., Calvert, A. T., & Graham, S. A. (2009). Age, geochemical composition, and distribution of Oligocene ignimbrites in the northern Sierra Nevada, California: Implications for landscape morphology, elevation, and drainage divide geography of the Nevadaplano. *International Geology Review*, 51(7–8), 723–742. <https://doi.org/10.1080/00206810902880370>
- Castelltort, S., Whittaker, A. C., & Vergés, J. (2015). Tectonics, sedimentation and surface processes: From the erosional engine to basin deposition. *Earth Surface Processes and Landforms*, 40(13), 1839–1846. <https://doi.org/10.1002/esp.3769>
- Cather, S. M., Connell, S. D., Chamberlin, R. M., McIntosh, W. C., Jones, G. E., Potocznik, A. R., et al. (2008). The Chuska erg: Paleogeomorphic and paleoclimatic implications of an Oligocene sand sea on the Colorado Plateau. *GSA Bulletin*, 120(1–2), 13–33.
- Chamberlain, C. P., Mix, H. T., Mulch, A., Hren, M. T., Kent-Corson, M. L., Davis, S. J., et al. (2012). The Cenozoic climatic and topographic evolution of the western north American Cordillera. *American Journal of Science*, 312(2), 213–262. <https://doi.org/10.2475/02.2012.05>
- Channer, M. A., Ricketts, J. W., Zimmerer, M., Heizler, M., & Karlstrom, K. E. (2015). Surface uplift above the Jemez mantle anomaly in the past 4 Ma based on  $^4\text{Ar}/^{39}\text{Ar}$  dated paleoprofiles of the Rio San Jose, New Mexico, USA. *Geosphere*, 11(5), 1384–1400. <https://doi.org/10.1130/GES01145.1>
- Chapin, C. E., Wilks, M., & McIntosh, W. C. (2004). Space-time patterns of Late Cretaceous to present magmatism in New Mexico—Comparison with Andean volcanism and potential for future volcanism. *New Mexico Bureau Geography and Mineral Resources Bulletin*, 160, 13–40.
- Colgan, J. P., & Henry, C. D. (2009). Rapid middle Miocene collapse of the Mesozoic orogenic plateau in north-central Nevada. *International Geology Review*, 51(9–11), 920–961. <https://doi.org/10.1080/00206810903056731>
- Croissant, T., & Braun, J. (2014). Constraining the stream power law: A novel approach combining a landscape evolution model and an inversion method. *Earth Surface Dynamics*, 2, 155–166.
- Crosby, B. T., & Whipple, K. X. (2006). Knickpoint initiation and distribution within fluvial networks, 236 waterfalls in the Waipaoa River, North Island, New Zealand. *Geomorphology*, 82, 16–38. <https://doi.org/10.1016/j.geomorph.2005.08.023>
- Cross, T. A. (1986). Tectonic controls of foreland basin subsidence and Laramide style deformation, western United States. *Foreland basins* (pp. 13–39). <https://doi.org/10.1002/9781444303810.ch1>
- Cross, T. A., & Pilger, R. H. (1978). Tectonic controls of late Cretaceous sedimentation, western interior, USA. *Nature*, 274, 653–657.
- Czarnota, K., Roberts, G. G., White, N. J., & Fishwick, S. (2014). Spatial and temporal patterns of Australian dynamic topography from river profile modeling. *Journal of Geophysical Research: Solid Earth*, 119, 1384–1424. <https://doi.org/10.1002/2013JB010436>
- Dávila, F. M., & Lithgow-Bertelloni, C. (2015). Dynamic uplift during slab flattening. *Earth and Planetary Science Letters*, 425, 34–43. <https://doi.org/10.1016/j.epsl.2015.05.026>
- Davis, W. M. (1899). The geographical cycle. *Geochemical Journal*, 14(5), 481–504. <https://doi.org/10.1086/521238>
- DeCelles, P. G. (1994). Late Cretaceous-Paleocene synorogenic sedimentation and kinematic history of the Sevier thrust belt, northeast Utah and southwest Wyoming. *GSA Bulletin*, 106(1), 32–56.
- DeCelles, P. G. (2004). Late Jurassic to Eocene evolution of the Cordilleran thrust belt and foreland basin system, Western U.S.A. *American Journal of Science*, 304, 105–168. <https://doi.org/10.2475/ajs.304.2.105>
- DiBiase, R. A., Whipple, K. X., Lamb, M. P., & Heimsath, A. M. (2014). The role of waterfalls and knickzones in controlling the style and pace of landscape adjustment in the western San Gabriel Mountains, California. *Bulletin Geological Society of America*, 127(3–4), 539–559. <https://doi.org/10.1130/B31113.1>
- Dickie, K., Keen, C. E., Williams, G. L., & Dehler, S. A. (2011). Tectonostratigraphic evolution of the Labrador margin, Atlantic Canada. *Marine and Petroleum Geology*, 28, 1663–1675. <https://doi.org/10.1016/j.marpetgeo.2011.05.009>
- Dickinson, W. R. (2004). Evolution of the North American Cordillera. *Annual Review of Earth and Planetary Sciences*, 32(1), 13–45. <https://doi.org/10.1146/annurev.earth.32.101802.120257>
- Dickinson, W. R., Klute, M. A., Hayes, M. J., Janecke, S. U., Lundin, E. R., McKittrick, M. A., & Olivares, M. D. (1988). Paleogeographic and paleotectonic setting of Laramide sedimentary basins in the central Rocky Mountain region. *Bulletin Geological Society of America*, 100(7), 1023–1039. [https://doi.org/10.1130/0016-7606\(1988\)100<1023:PAPSOL>2.3.CO;2](https://doi.org/10.1130/0016-7606(1988)100<1023:PAPSOL>2.3.CO;2)
- Dickinson, W. R., & Snyder, W. S. (1978). Plate tectonics of the Laramide orogeny. In I. I. I. Matthews Vincent (Ed.), *Laramide Fold Assoc. with Basement Block Faulting West. United States*. America: Geological Society of America.
- Dodson, M. H. (1973). Closure temperatures in cooling geological and petrological systems. *Contributions to Mineralogy and Petrology*, 40, 259–274.
- Dorsey, R. J., O'Connell, B., McDougall, K., & Homan, M. B. (2018). Punctuated sediment discharge during Early Pliocene birth of the Colorado River: Evidence from regional stratigraphy, sedimentology, and paleontology. *Sedimentary Geology*, 363, 1–33. <https://doi.org/10.1016/j.sedgeo.2017.09.018>
- Duller, R. A., Whittaker, A. C., Swinehart, J. B., Armitage, J. J., Sinclair, H. D., Bair, A., & Allen, P. A. (2012). Abrupt landscape change post-6 Ma on the central Great Plains, USA. *Geology*, 40(10), 871–874. <https://doi.org/10.1130/G32919.1>
- Fan, M., & Carrapa, B. (2014). Late Cretaceous-early Eocene Laramide uplift, exhumation, and basin subsidence in Wyoming: Crustal responses to flat slab subduction. *Tectonics*, 33, 509–529. <https://doi.org/10.1002/2012TC003221>
- Farley, K. A. (2002). (U-Th)/He dating: Techniques, calibrations, and applications. *Reviews in Mineralogy and Geochemistry*, 47(1), 819–844.
- Feng, J., Buffler, R. T., & Komink, M. A. (1994). Laramide orogenic influence on late Mesozoic-Cenozoic subsidence history, western deep Gulf of Mexico basin. *Geology*, 22(4), 359–362.
- Fenneman, N. (1928). Physiographic Divisions of the United States. *Annals of the Association of American Geographers*, 18(4), 261–353.
- Ferrari, L., & Bryan, S. (2007). Magmatism and tectonics of the Sierra Madre Occidental and its relation with the evolution of the western margin of North America. *Geological Society of America*, 2422(01), 1–39. [https://doi.org/10.1130/2007.2422\(01\)1-39](https://doi.org/10.1130/2007.2422(01)1-39)

- Ferrari, L., López-Martínez, M., Aguirre-Díaz, G., & Carrasco-Núñez, G. (1999). Space-time patterns of Cenozoic arc volcanism in central Mexico: From the Sierra Madre Occidental to the Mexican Volcanic Belt. *Geology*, 27(4), 303–306.
- Ferrari, L., López-Martínez, M., & Rosas-Elguera, J. (2002). Ignimbrite flare-up and deformation in the southern Sierra Madre\Occidental, western Mexico: Implications for the late subduction history of the Farallon plate. *Tectonics*, 21(4), 17–1–17–25. <https://doi.org/10.1029/2001TC001302>
- Ferrari, L., Orozco-Esquivel, T., Manea, V., & Manea, M. (2012). The dynamic history of the Trans-Mexican Volcanic Belt and the Mexico subduction zone. *Tectonophysics*, 522–523, 122–149. <https://doi.org/10.1016/j.tecto.2011.09.018>
- Fitton, J. G., James, D., & Leeman, W. P. (1991). Basic magmatism associated with Late Cenozoic extension in the western United States: Compositional variations in space and time. *Journal of Geophysical Research*, 96(B8), 13,693–13,711. <https://doi.org/10.1029/91JB00372>
- Flament, N., Gurnis, M., Müller, R. D., Bower, D. J., & Husson, L. (2015). Influence of subduction history on South American topography. *Earth and Planetary Science Letters*, 430, 9–18. <https://doi.org/10.1016/j.epsl.2015.08.006>
- Flowers, R. M., Ault, A. K., Kelley, S. A., Zhang, N., & Zhong, S. (2012). Apatite 4He/3He and (U-Th)/He evidence for an ancient Grand Canyon. *Science*, 338, 1616–1619. <https://doi.org/10.1126/science.1229390>
- Flowers, R. M., & Farley, K. A. (2012). Apatite 4He/3He and (U-Th)/He evidence for an ancient Grand Canyon. *Science*, 338, 1616–1619. <https://doi.org/10.1126/science.1229390>
- Flowers, R. M., Wernicke, B. P., & Farley, K. A. (2008). Unroofing, incision, and uplift history of the southwestern Colorado Plateau from apatite (U-Th)/He thermochronometry. *Bulletin Geological Society of America*, 120(5–6), 571–587. <https://doi.org/10.1130/B26231.1>
- Forte, A. M., Moucha, R., Simmons, N. A., Grand, S. P., & Mitrovica, J. X. (2009). Deep-mantle contributions to the surface dynamics of the North American continent. *Tectonophysics*, 481(1–4), 3–15. <https://doi.org/10.1016/j.tecto.2009.06.010>
- Forte, A. M., & Whipple, K. X. (2018). Criteria and tools for determining drainage divide stability. *Earth and Planetary Science Letters*, 493, 102–117.
- Fox, M., Goren, L., May, D. A., & Willett, S. D. (2014). Inversion of fluvial channels for paleorock uplift rates in Taiwan. *Journal of Geophysical Research: Earth Surface*, 119, 1853–1875. <https://doi.org/10.1002/2014JF003196>
- Fox, M., Herman, F., Willett, S. D., & May, D. A. (2014). A linear inversion method to infer exhumation rates in space and time from thermochronometric data. *Earth Surface Dynamics*, 2(1), 47–65. <https://doi.org/10.5194/esurf-2-47-2014>
- French, S., Lekic, V., & Romanowicz, B. (2013). Waveform tomography reveals channeled flow at the base of the oceanic lithosphere. *Science*, 342(6359), 277–230. <https://doi.org/10.1126/science.1229370>
- Gallagher, K. (1995). Evolving temperature histories from apatite fission-track data. *Earth and Planetary Science Letters*, 136(3–4), 421–435. [https://doi.org/10.1016/0012-821X\(95\)00197-K](https://doi.org/10.1016/0012-821X(95)00197-K)
- Gallagher, K. (2012). Transdimensional inverse thermal history modeling for quantitative thermochronology. *Journal of Geophysical Research*, 117, B02408. <https://doi.org/10.1029/2011JB008825>
- Gallen, S. F. (2018). Lithologic controls on landscape dynamics and aquatic species evolution in post-orogenic mountains. *Earth and Planetary Science Letters*, 493, 150–160.
- Gallen, S. F., Wegmann, K. W., & Bohnenstiehl, D. W. R. (2013). Miocene rejuvenation of topographic relief in the southern Appalachians. *GSA Today*, 23(2), 4–10. <https://doi.org/10.1130/GSATG163A.1>
- Galloway, W. E. (2001). Cenozoic evolution of sediment accumulation in deltaic and shore-zone depositional systems, Northern Gulf of Mexico Basin. *Marine and Petroleum Geology*, 18(10), 1031–1040. [https://doi.org/10.1016/S0264-8172\(01\)00045-9](https://doi.org/10.1016/S0264-8172(01)00045-9)
- Galloway, W. E. (2008). Depositional evolution of the Gulf of Mexico sedimentary basin. In Galloway, W. E. (Ed.), *Sedimentary basins world* (Vol. 5, pp. 505–549). Mexico: Elsevier. [https://doi.org/10.1016/S1874-5997\(08\)00015-4](https://doi.org/10.1016/S1874-5997(08)00015-4)
- Galloway, W., Ganey-Curry, P., Li, X., & Buffler, R. T. (2000). Cenozoic depositional history of the Gulf of Mexico basin. *American Association of Petroleum Geologists Bulletin*, 84(11), 1743–1774. <https://doi.org/10.1306/110801720476>
- Galloway, W. E., Whiteaker, T. L., & Ganey-Curry, P. (2011). History of Cenozoic North American drainage basin evolution, sediment yield, and accumulation in the Gulf of Mexico basin. *Geosphere*, 7(4), 938–973. <https://doi.org/10.1130/GES00647.1>
- Gani, R. M., Ranson, A., Cross, D. B., Hampson, G. J., Gani, N. D., & Sahoo, H. (2015). Along-strike sequence stratigraphy across the Cretaceous shallow marine to coastal-plain transition, Wasatch Plateau, Utah, U.S.A. *Sedimentary Geology*, 325, 59–70.
- Gans, P. B., & Miller, E. L. (1983). Style of mid-Tertiary extension in east-central Nevada. *Geology excursions overthrust belt Metamorphic core complexes Intermittent Regulation of Utah Geological and Mineral Survey Special Studies*, 59, 107–139.
- Gilbert, G. K. (1877). *Report on the geology of the Henry Mountains, Geological Survey of the Rocky Mountains*. U.S: Department of the Interior.
- Gleadow, A. J. W., & Brown, R. W. (1999). Fission track thermochronology and the long-term denudational response to tectonics. *Geomorphology and Global Tectonics*, 12, 57–75.
- Glotzbach, C. (2015). Deriving rock uplift histories from data-driven inversion of river profiles. *Geology*, 43, 467–470.
- Gohn, G. S. (1988). Late Mesozoic and early Cenozoic geology of the Atlantic Coastal Plain: North Carolina to Florida. In Sheridan, R. E., & Grow, J. A. (Eds.), *Atl. Cont. Margin U.S.* (Vol. I-2, pp. 107–130), *The Geology of North America*. Boulder, CO: Geological Society of America.
- Goren, L., Willett, S. D., Herman, F., & Braun, J. (2014). Coupled numerical-analytical approach to landscape evolution modeling. *Earth Surface Processes and Landforms*, 39(4), 522–545. <https://doi.org/10.1002/esp.3514>
- Gradstein, F. M., Ogg, J. G., & Frits, F. J. (2012). On the geological timescale. *Newsletters on Stratigraphy*, 2, 171–188. <https://doi.org/10.1127/0078-0421/2012/0020>
- Gray, G. G., Pottorf, R. J., Yurewicz, D. A., Mahon, K. I., Pevear, D. R., & Chuchla, R. J. (2001). Thermal and chronological record of syn- to post-Laramide burial and exhumation, Sierra Madre Oriental, Mexico. In C. Bartolini, R. T. Buffler, & A. Cantu-Chapa (Eds.), *AAPG memoir: The Western Gulf of Mexico Basin: Tectonics, sedimentary basins, and petroleum systems* (Vol. 75, pp. 159–181). America: AAPG.
- Green, P. F., Duddy, I. R., Gleadow, A. J., & Lovering, J. F. (1989). Apatite fission-track analysis as a paleotemperature indicator for hydrocarbon exploration. In N. D. Naeser, & T. H. McCulloh (Eds.), *Therm. Hist. Sediment. Basins*. New York: Springer. [https://doi.org/10.1007/978-1-4612-3492-0\\_11](https://doi.org/10.1007/978-1-4612-3492-0_11)
- Greenwood, D. R., & Wing, S. L. (1995). Eocene continental climates and latitudinal temperature gradients. *Geology*, 23, 1044–1048.
- Gregory, K. M., & Chase, C. G. (1992). Tectonic significance of paleobotanically estimated climate and altitude of the late Eocene erosion surface, Colorado. *Geology*, 20, 581–585.
- Gurnis, M. (1993). Phanerozoic marine inundation of continent driven by dynamic topography above subducting slabs. *Nature*, 364, 590–593.

- Gurnis, M., Mitrovica, J. X., Ritsema, J., & van Heijst, H. J. (2000). Constraining mantle density structure using geological evidence of surface uplift rates: The case of the African Superplume. *Geochemistry, Geophysics, Geosystems*, 1(7). <https://doi.org/10.1029/1999GC000035>
- Heaman, L. M., Kjarsgaard, B. A., & Creaser, R. A. (2004). The temporal evolution of North American kimberlites. *Lithos*, 76, 377–397. <https://doi.org/10.1016/j.lithos.2004.03.047>
- Heller, P. L., & Liu, L. (2016). Dynamic topography and vertical motion of the U.S. Rocky Mountain region prior to and during the Laramide orogeny. *Geological Society of America Bulletin*, 128(5–6), 973–988. <https://doi.org/10.1130/B31431.1>
- Heller, P. L., Mathers, G., Dueker, K., & Foreman, B. (2013). Far-traveled latest Cretaceous-Paleocene conglomerates of the Southern Rocky Mountains, USA: Record of transient Laramide tectonism. *Bulletin Geological Society of America*, 125(3–4), 490–498. <https://doi.org/10.1130/B30699.1>
- Henry, C. D., Hinz, N. H., Faulds, J. E., Colgan, J. P., John, D. A., Brooks, E. R., et al. (2012). Eocene-Early Miocene paleotopography of the Sierra Nevada-Great Basin-Nevadaplano based on widespread ash-flow tuffs and paleovalleys. *Geosphere*, 8, 1–27. <https://doi.org/10.1130/GES00727.1>
- Herman, F., & Braun, J. (2006). Fluvial response to horizontal shortening and glaciations: A study in the Southern Alps of New Zealand. *Journal of Geophysical Research*, 111, F01008. <https://doi.org/10.1029/2004JF000248>
- Herman, F., Seward, D., Valla, P. G., Carter, A., Kohn, B., Willett, S. D., & Ehlers, T. (2013). Worldwide acceleration of mountain erosion under a cooling climate. *Nature*, 504(7480), 423–426. <https://doi.org/10.1038/nature12877>
- Hoggard, M. J., White, N., & Al-Attar, D. (2016). Global dynamic topography observations reveal limited influence of large-scale mantle flow. *Nature Geoscience*, 9, 456.
- Hosman, R. L. (1996). Regional stratigraphy and subsurface geology of Cenozoic deposits, Gulf Coastal Plain, south-central United States: U.S. Geological Survey Professional Paper 1416-G. 1–35.
- Howard, A. D. (1994). A detachment-limited model of drainage basin evolution. *Water Resources Research*, 30, 2261–2285.
- Howard, A. D., & Kerby, G. (1983). Channel changes in badlands. *Geological Society of America Bulletin*, 94, 739–752.
- Humphreys, E. D. (1995). Post-Laramide removal of the Farallon slab, western United States. *Geology*, 23(13), 987–990. [https://doi.org/10.1130/0091-7613\(1995\)023<0987](https://doi.org/10.1130/0091-7613(1995)023<0987)
- Humphreys, E. D., Hessler, E., Dueker, K., Farmer, G. L., Erslev, E., & Atwater, T. (2003). How Laramide-age hydration of North American lithosphere by the Farallon slab controlled subsequent activity in the western United States. *International Geology Review*, 45(7), 575–595. <https://doi.org/10.2747/0020-6814.45.7.575>
- Huntington, K. W., Wernicke, B. P., & Eiler, J. M. (2010). Influence of climate change and uplift on Colorado Plateau paleotemperatures from carbonate clumped isotope thermometry. *Tectonics*, 29, TC3005. <https://doi.org/10.1029/2009TC002449>
- Immenhauser, A. (2009). Estimating palaeo-water depth from the physical rock record. *Earth-Science Reviews*, 96(1–2), 107–139. <https://doi.org/10.1016/j.earscirev.2009.06.003>
- Japsen, P., Green, P. F., Bonow, J. M., Hinckley, A. M., & Wilton, D. H. C. (2016). Burial and exhumation history of the Labrador-Newfoundland margin: First observations. *Geological Survey of Denmark and Greenland Bulletin*, 35, 91–94.
- Jeletzky, J. A. (1971). Marine Cretaceous biotic province and paleogeography of western and arctic Canada: Illustrated by a detailed study of ammonites. *Geological Survey of Canada*, 70, 1–92.
- Johnson, K. R., Nichols, D. J., & Hartman, J. H. (2002). Hell Creek Formation: A 2001 synthesis, in, The Hell Creek Formation and the Cretaceous-Tertiary boundary in the northern Great Plains: An integrated continental record of the end of the Cretaceous. In J. H. Hartman, K. R. Johnson, & D. J. Nichols (Eds.), *Geological Society of America Special Paper* (pp. 503–510).
- Johnston, S. T. (2001). The Great Alaskan Terrane Wreck: Reconciliation of paleomagnetic and geological data in the Northern Cordillera. *Earth and Planetary Science Letters*, 193, 25–272.
- Karlstrom, K. E., Coblenz, D., Dueker, K., Ouimet, W., Kirby, E., Van Wijk, J. W., et al. (2012). Mantle-driven dynamic uplift of the Rocky Mountains and Colorado Plateau and its surface response: Toward a unified hypothesis. *Lithosphere*, 4(1), 3–22. <https://doi.org/10.1130/L150.1>
- Karlstrom, K. E., Crossey, L. J., Embid, E., Crow, R., Heizler, M., Hereford, R., et al. (2017). Cenozoic incision history of the Little Colorado River: Its role in carving Grand Canyon and onset of rapid incision in the past ca. 2 Ma in the Colorado River System. *Geosphere*, 13(1), 49–81. <https://doi.org/10.1130/GES01304.1>
- Karlstrom, K. E., Crow, R. S., Crossey, L. J., Coblenz, D., & Van Wijk, J. W. (2008). Model for tectonically driven incision of the younger than 6 Ma Grand Canyon. *Geology*, 36(11), 835–838. <https://doi.org/10.1130/G25032A.1>
- Karlstrom, K. E., Lee, J. P., Kelley, S. A., Crow, R. S., Crossey, L. J., Young, R. A., et al. (2014). Formation of the Grand Canyon 5 to 6 million years ago through integration of older palaeocanyons. *Nature Geoscience*, 7(3), 239–244. <https://doi.org/10.1038/ngeo2065>
- Kauffman, E. G., & Caldwell, W. G. E. (1993). The Western Interior Basin in space and time. *GAC Special Publication*, 39(2), 1–30.
- Kelley, S. A., & Chapin, C. E. (1995). Apatite fission-track thermochronology of the southern Rocky Mountain-Rio Grande rift-western High Plains province. *New Mexico Geological Society Field Conference Guidebook*, 46, 87–96.
- Ketcham, R. A. (2005). Forward and inverse modeling of low-temperature thermochronometry data. *Reviews in Mineralogy and Geochemistry*, 58(1), 275–314. <https://doi.org/10.2138/rmg.2005.58.11>
- Kirby, E., & Whipple, K. (2001). Quantifying differential rock-uplift rates via stream profile analysis. *Geology*, 29, 415–418.
- Clitord, K. D., Hutchinson, D. R., & Schouten, H. (1988). U.S. Atlantic continental margin: Structural and tectonic framework. In R. E. Sheridan, & J. E. Grow (Eds.), *Atl. Cont. Margin U.S. (Vol. I-2)*, *The Geology of North America*. Boulder, CO: Geological Society of America.
- Klocking, M., White, N. J., MacLennan, J., McKenzie, D., & Fitton, J. G. (2018). Quantitative relationships between basalt geochemistry, shear wave velocity and asthenospheric temperature beneath western North America. *Geochemistry, Geophysics, Geosystems*, 19, 3376–3404. <https://doi.org/10.1029/2018GC007559>
- Koppes, M. N., & Montgomery, D. R. (2009). The relative efficacy of fluvial and glacial erosion over modern to orogenic timescales. *Nature Geoscience*, 2, 644–647.
- Lague, D. (2014). The stream power river incision model: Evidence, theory and beyond. *Earth Surface Processes and Landforms*, 39(1), 38–61. <https://doi.org/10.1002/esp.3462>
- Lague, D., Crave, A., & Davy, P. (2003). Laboratory experiments simulating the geomorphic response to tectonic uplift. *Journal of Geophysical Research*, 108(B1), 2008. <https://doi.org/10.1029/2002JB001785>
- Levander, A., & Miller, M. S. (2012). Evolutionary aspects of lithosphere discontinuity structure in the Western U.S. *Geochemistry, Geophysics, Geosystems*, 13, Q0AK07. <https://doi.org/10.1029/2012GC004056>
- Levandowski, W., Jones, C. H., Butcher, L. A., & Mahan, K. H. (2018). Lithospheric density models reveal evidence for Cenozoic uplift of the Colorado Plateau and Great Plains by lower-crustal hydration. *Geosphere*, 14(3), 1–15. <https://doi.org/10.1130/GES01619.1>

- Lillegraven, J. A., & Ostresh, L. M. (1988). Evolution of Wyoming Early Cenozoic topography and drainage patterns. *National Geographic Research*, 4(3), 303–327.
- Lisker, F., Ventura, B., & Glasmacher, U. A. (2009). Apatite thermochronology in modern geology. *Geological Society of London, Special Publication*, 324(1–15), 1–23.
- Lithgow-Bertelloni, C., & Gurnis, M. (1997). Cenozoic subsidence and uplift of continents from time-varying dynamic topography. *Geology*, 25(8), 735–738. [https://doi.org/10.1130/0091-7613\(1997\)025<0735](https://doi.org/10.1130/0091-7613(1997)025<0735)
- Liu, L. (2014). Rejuvenation of Appalachian topography caused by subsidence-induced differential erosion. *Nature Geoscience*, 7, 518–523. <https://doi.org/10.1038/ngeo2187>
- Liu, L. (2015). The ups and downs of North America: Evaluating the role of mantle dynamic topography since the Mesozoic. *Reviews of Geophysics*, 53, 1022–1049. <https://doi.org/10.1002/2015RG000489>
- Liu, L., & Gurnis, M. (2010). Dynamic subsidence and uplift of the Colorado Plateau. *Geology*, 38(7), 663–666. <https://doi.org/10.1130/G30624.1>
- Liu, S., & Nummedal, D. (2004). Late Cretaceous subsidence in Wyoming: Quantifying the dynamic component. *Geology*, 32(5), 397–400. <https://doi.org/10.1130/G20318.1>
- Liu, L., Spasojević, S., & Gurnis, M. (2008). Reconstructing Farallon plate subduction beneath North America back to the Late Cretaceous. *Science*, 322, 934–938. <https://doi.org/10.1126/science.1165110>
- Lodhia, B. H., Roberts, G. G., Fraser, A. J., Fishwick, S., Goes, S., & Jarvis, J. (2018). Continental margin subsidence from shallow mantle convection: Example from West Africa. *Earth and Planetary Science Letters*, 481, 350–361. <https://doi.org/10.1016/j.epsl.2017.10.024>
- Loget, N., & Van Den Driessche, J. (2009). Wave train model for knickpoint migration. *Geomorphology*, 106(3–4), 376–382. <https://doi.org/10.1016/j.geomorph.2008.10.017>
- Luke, J. C. (1972). Mathematical models for landform evolution. *Journal of Geophysical Research*, 77(14), 2460–2464.
- Mackey, B. H., Scheingross, J. S., Lamb, M. P., & Farley, K. A. (2014). Knickpoint formation, rapid propagation, and landscape response following coastal cliff retreat at the last interglacial sea-level highstand: Kaua'i, Hawai'i. *Bulletin Geological Society of America*, 126(7–8), 925–942. <https://doi.org/10.1130/B30930.1>
- Marquez, A., Oyarzun, R., Doblas, M., & Verma, S. P. (1999). Alkalic (ocean-island basalt type) and calc-alkalic volcanism in the Mexican volcanic belt: A case for plume-related magmatism and propagating rifting at an active margin? *Geology*, 27(1), 51–54.
- Matmon, A., Bierman, P. R., Larsen, J., Southworth, S., Pavich, M., & Caffee, M. (2003). Temporally and spatially uniform rates of erosion in the southern Appalachian Great Smoky Mountains. *Geology*, 31(2), 155–158. [https://doi.org/10.1130/0091-7613\(2003\)031<0155:TASURO>2.0.CO;2](https://doi.org/10.1130/0091-7613(2003)031<0155:TASURO>2.0.CO;2)
- McKenna, M. C., & Love, J. D. (1972). High-level strata containing Early Miocene mammals on the Bighorn Mountains, Wyoming. *American Museum Novitates*, 2490, 31.
- McKenzie, D. (2003). Estimating  $T_e$  in the presence of internal loads. *Journal of Geophysical Research*, 108(B9), 2438. <https://doi.org/10.1029/2002JB001766>
- McKenzie, D., Jackson, J., & Priestley, K. (2005). Thermal structure of oceanic and continental lithosphere. *Earth and Planetary Science Letters*, 233(3–4), 337–349. <https://doi.org/10.1016/j.epsl.2005.02.005>
- McKeon, R. E., Zeitzer, P. K., Pazzaglia, F. J., Idleman, B. D., & Enkelmann, E. (2014). Decay of an old orogen: Inferences about Appalachian landscape evolution from low-temperature thermochronology. *Bulletin Geological Society of America*, 126(1–2), 31–46. <https://doi.org/10.1130/B30808.1>
- McMillan, M. E., Angevine, C. L., & Heller, P. L. (2002). Postdepositional tilt of the Miocene-Pleistocene Ogallala Group on the western Great Plains: Evidence of Late Cenozoic uplift of the Rocky Mountains. *Geological Society of America*, 30, 63–66.
- McMillan, M. E., Heller, P. L., & Wing, S. L. (2006). History and causes of post-Laramide relief in the Rocky Mountain orogenic plateau. *Bulletin Geological Society of America*, 118(3–4), 393–405. <https://doi.org/10.1130/B25712.1>
- McQuarrie, N., & Chase, C. G. (2000). Raising the Colorado Plateau; discussion and reply. *Geology*, 28(8), 767–768. [https://doi.org/10.1130/0091-7613\(2000\)028<0091:RTCP>2.0.CO;2](https://doi.org/10.1130/0091-7613(2000)028<0091:RTCP>2.0.CO;2)
- Menke, W., Skryzalin, P., Levin, V., Harper, T., Darbyshire, F., & Dong, T. (2016). The Northern Appalachian Anomaly: A modern asthenospheric upwelling. *Geophysical Research Letters*, 43, 10,173–10,179. <https://doi.org/10.1002/2016GL070918>
- Merewether, E. A., & McKinney, K. C. (2015). Composite biostratigraphic outcrop sections for Cretaceous Formations along a south-trending transect from northwestern Montana to northwestern New Mexico. *USGS*, 1258, 20151, 087.
- Miller, K. G. (2005). The Phanerozoic record of global sea-level change. *Science*, 310(5752), 1293–1298. <https://doi.org/10.1126/science.1116412>
- Miller, S. R., Sak, P. B., Kirby, E., & Bierman, P. R. (2013). Neogene rejuvenation of central Appalachian topography: Evidence for differential rock uplift from stream profiles and erosion rates. *Earth and Planetary Science Letters*, 369–370, 1–12. <https://doi.org/10.1016/j.epsl.2013.04.007>
- Milliken, K. T., Blum, M. D., Snedden, J. W., & Galloway, W. E. (2018). Application of fluvial scaling relationships to reconstruct drainage basin evolution and sediment routing for the Cretaceous and Paleocene of the Gulf of Mexico. *Geosphere*, 14(2), 749–767. <https://doi.org/10.1130/GES01374.1>
- Missimer, T. M., & Maliva, R. G. (2017). Late Miocene fluvial sediment transport from the southern Appalachian Mountains to southern Florida: An example of an old mountain belt sediment production surge. *Sedimentology*, 64(7), 1846–1870. <https://doi.org/10.1111/sed.12377>
- Mitrovica, J. X., Beaumont, C., & Jarvis, G. T. (1989). Tilting of continental interiors by the dynamical effects of subduction. *Tectonics*, 8(5), 1079–1094. <https://doi.org/10.1029/TC008i005p01079>
- Mix, H. T., Mulch, A., Kent-Corson, M. L., & Chamberlain, C. P. (2011). Cenozoic migration of topography in the North American Cordillera. *Geology*, 39(1), 87–90. <https://doi.org/10.1130/G31450.1>
- Molnar, P., England, P. C., & Jones, C. H. (2015). Mantle dynamics, isostasy, and the support of high terrain. *Journal of Geophysical Research: Solid Earth*, 120, 1932–1957. <https://doi.org/10.1002/2014JB011724>
- Montgomery, D. R., & López-Blanco, J. (2003). Post-Oligocene river incision, southern Sierra Madre Occidental, Mexico. *Geomorphology*, 55(1–4), 235–247. [https://doi.org/10.1016/S0169-555X\(03\)00142-9](https://doi.org/10.1016/S0169-555X(03)00142-9)
- Moucha, R., Forte, A. M., Mitrovica, J. X., Rowley, D. B., Quéré, S., Simmons, N. A., & Grand, S. P. (2016). Dynamic topography and long-term sea-level variations: There is no such thing as a stable continental platform. *Earth and Planetary Science Letters*, 271(1–4), 101–108.
- Naeser, C. W., Naeser, N. D., Newell, W. L., Southworth, S., Edwards, L. E., & Weems, R. E. (2016). Erosional and depositional history of the Atlantic passive margin as recorded in detrital zircon fission-track ages and lithic detritus in Atlantic Coastal Plain sediments. *American Journal of Science*, 316(2), 110–168. <https://doi.org/10.2475/02.2016.02>

- Naeser, N. D., Naeser, C. W., Southworth, C. S., Morgan, B. A., & Schultz, A. P. (2004). Paleozoic to Recent tectonic and denudation history of rocks in the Blue Ridge Province, central and southern Appalachians—Evidence from fission-track thermochronology. *Geological Society of America Abstracts with Programs*, 36(2), 114.
- Nassichuk, W. W., & McIntyre, D. J. (1995). Cretaceous and Tertiary fossils discovered in kimberlites at Lac de Gras in the Slave Province, Northwest Territories. *Curriculum Research - Geological Survey of Canada*, B, 109–114.
- Nereson, A., Stroud, J., Karlstrom, K., Heizler, M., & McIntosh, W. (2013). Dynamic topography of the western Great Plains: Geomorphic and  $^{40}\text{Ar}/^{39}\text{Ar}$  evidence for mantle-driven uplift associated with the Jemez lineament of NE New Mexico and SE Colorado. *Geosphere*, 9(3), 521–545. <https://doi.org/10.1130/GES00837.1>
- Nurkowski, J. R. (1984). Coal quality, coal rank variation and its relation to reconstructed overburden, Upper Cretaceous and Tertiary plains coals, Alberta, Canada. *American Association of Petroleum Geologists Bulletin*, 68(3), 285–295.
- O'Sullivan, P. B., & Currie, L. D. (1996). Thermotectonic history of Mt Logan, Yukon Territory, Canada: Implications of multiple episodes of middle to late Cenozoic denudation. *Earth and Planetary Science Letters*, 144, 251–261.
- O'Sullivan, P. B., & Lane, L. S. (1997). Early Tertiary thermotectonic history of the northern Yukon and adjacent Northwest Territories, Arctic Canada. *Canadian Journal of Earth Sciences*, 34(10), 1366–1378. <https://doi.org/10.1139/e17-109>
- Obradovich, J. D., & Cobban, W. A. (1975). A time-scale for the Late Cretaceous of the Western Interior of North America. *Geological Association of Canada Special Paper*, 13, 31–54.
- Olsson, R. K., Gibson, T. G., Hansen, H. J., & Owens, J. P. (1988). Geology of the northern Atlantic coastal plain: Long Island to Virginia. In R. E. Sheridan, & J. A. Grow (Eds.), *Atl. Cont. Margin U.S. (Vol. I-2, pp. 87–105)*, *The Geology of North America*. Boulder, CO: Geological Society of America.
- Pang, M., & Nummedal, D. (1995). Flexural subsidence and basement tectonics of the Cretaceous Western Interior basin, United States. *Geology*, 23(2), 173–176.
- Parker, R. L. (1994). *Geophysical inverse theory*. New Jersey: Princeton University Press.
- Paul, J. D., Roberts, G. G., & White, N. (2014). The African landscape through space and time. *Tectonics*, 33, 898–935. <https://doi.org/10.1002/2013TC003479>
- Pavich, M. J., Brown, L., Valette-Silver, J. N., Klein, J., & Middleton, R. (1985).  $^{10}\text{Be}$  analysis of a Quaternary weathering profile in the Virginia Piedmont. *Geology*, 13(1), 39–41.
- Pazzaglia, F. J., & Brandon, M. T. (1996). Macrogeomorphic evolution of the post-Triassic Appalachian mountains determined by deconvolution of the offshore basin sedimentary record. *Basin Research*, 8(1996), 1–24.
- Pazzaglia, F. J., & Gardner, W. (1994). Late Cenozoic flexural deformation of the middle U.S. Atlantic passive margin. *Journal of Geodynamics*, 99(B6), 12143–12157.
- Peel, F. J., Travis, C. J., & Hossback, J. R. (1995). Genetic structural provinces and salt tectonics of the Cenozoic offshore U.S. Gulf of Mexico: A preliminary analysis. In F. J. Peel, C. J. Travis, & J. R. Hossback (Eds.), *Salt tectonics a Global Perspective* pp. 153–175). Mexico: AAPG Memoir.
- Peyton, S. L., & Carrapa, B. (2013). An overview of low-temperature thermochronology in the Rocky Mountains and its application to petroleum system analysis. *AAPG Studies in Geology*, 65, 37–70. <https://doi.org/10.1306/13381689St653578>
- Poag, C. W., & Sevon, W. D. (1989). A record of Appalachian denudation in postrift Mesozoic and Cenozoic sedimentary deposits of the U.S. Middle Atlantic continental margin. *Geomorphology*, 2(1–3), 119–157. [https://doi.org/10.1016/0169-555X\(89\)90009-3](https://doi.org/10.1016/0169-555X(89)90009-3)
- Portenga, E. W., Bierman, P. R., Rizzo, D. M., & Rood, D. H. (2013). Low rates of bedrock outcrop erosion in the Central Appalachian mountains inferred from in situ  $^{10}\text{Be}$ . *Bulletin Geological Society of America*, 125(1–2), 201–215. <https://doi.org/10.1130/B30559.1>
- Priestley, K., & McKenzie, D. (2006). The thermal structure of the lithosphere from shear wave velocities. *Earth and Planetary Science Letters*, 244(1–2), 285–301. <https://doi.org/10.1016/j.epsl.2006.01.008>
- Prince, P. S., & Spotila, J. A. (2013). Evidence of transient topographic disequilibrium in a landward passive margin river system: Knickpoints and paleo-landscapes of the New River basin, southern Appalachians. *Earth Surface Processes and Landforms*, 38(14), 1685–1699. <https://doi.org/10.1002/esp.3406>
- Pritchard, D., Roberts, G. G., White, N. J., & Richardson, C. N. (2009). Uplift histories from river profiles. *Geophysical Research Letters*, 36, L24301. <https://doi.org/10.1029/2009GL040928>
- Ramirez-Herrera, M. T., Kostoglodov, V., & Urrutia-Fucugauchi, J. (2011). Overview of recent coastal tectonic deformation in the Mexican subduction zone. *Pure and Applied Geophysics*, 168(8–9), 1415–1433. <https://doi.org/10.1007/s0024-010-0205-y>
- Reed, J. C. Jr., Wheeler, J. O., & Tucholke, B. E. (2005). Geologic map of North America, Geol. Soc. Am., Geological Society of America Geology.
- Reiners, P. W., & Brandon, M. T. (2006). Using thermochronology to understand orogenic erosion. *Annual Review of Earth and Planetary Sciences*, 34, 419–466. <https://doi.org/10.1146/annurev.earth.34.031405.125202>
- Rengers, F. K., & Tucker, G. E. (2014). Analysis and modeling of gully headcut dynamics, North American high plains. *Journal of Geophysical Research: Earth Surface*, 119, 983–1003. <https://doi.org/10.1002/2013JF002962>
- Repasch, M., Karlstrom, K., Heizler, M., & Pecha, M. (2017). Birth and evolution of the Rio Grande fluvial system in the past 8 Ma: Progressive downward integration and the influence of tectonics, volcanism, and climate. *Earth-Science Review*, 168, 113–164. <https://doi.org/10.1016/j.earscirev.2017.03.003>
- Ritsema, J., Deuss, A., van Heijst, H. J., & Woodhouse, J. H. (2011). S40RTS: A degree-40 shear-velocity model for the mantle from new Rayleigh wave dispersion, teleseismic traveltimes and normal-mode splitting function measurements. *Geophysical Journal International*, 184(3), 1223–1236.
- Roberts, G. G. (2019). Scales of similarity and disparity between drainage networks. *Geophysical Research Letters*, 46, 3781–3790. <https://doi.org/10.1029/2019GL082446>
- Roberts, L. N., & Kirschbaum, M. A. (1995). Paleogeography of the Late Cretaceous of the Western Interior of middle North America—Coal distribution and sediment accumulation. *U.S. Geological Survey Professional Paper*, 1561, 115.
- Roberts, G. G., Paul, J. D., White, N., & Winterbourne, J. (2012). Temporal and spatial evolution of dynamic support from river profiles: A framework for Madagascar. *Geochemistry, Geophysics, Geosystems*, 13, Q04004. <https://doi.org/10.1029/2012GC004040>
- Roberts, G. G., & White, N. (2010). Estimating uplift rate histories from river profiles using African examples. *Journal of Geophysical Research*, 115, B02406. <https://doi.org/10.1029/2009JB006692>
- Roberts, G. G., White, N., Hoggard, M. J., Ball, P. W., & Meenan, C. (2018). A Neogene history of mantle convective support beneath Borneo. *Earth and Planetary Science Letters*, 496, 142–158. <https://doi.org/10.1016/j.epsl.2018.05.043>
- Roberts, G. G., White, N. J., & Lodhia, B. H. (2019). Generation and scaling of longitudinal river profiles. *Journal of Geophysical Research: Earth Surface*, 124, 137–153. <https://doi.org/10.1029/2018JF004796>

- Roberts, G. G., White, N. J., Martin-Brandis, G. L., & Crosby, A. G. (2012). An uplift history of the Colorado Plateau and its surroundings from inverse modeling of longitudinal river profiles. *Tectonics*, 31, TC4022. <https://doi.org/10.1029/2012TC003107>
- Roden-Tice, M. K., Eusden, J. D., & Wintsch, R. P. (2012). Apatite fission-track evidence for the Cretaceous development of kilometer-scale relief and steady-state Tertiary topography in New England. *Geomorphology*, 141–142, 114–120. <https://doi.org/10.1016/j.geomorph.2011.12.029>
- Rosenbloom, N. A., & Anderson, R. S. (1994). Hillslope and channel evolution in a marine terraced landscape, Santa Cruz, California. *Journal of Geophysical Research*, 99, 13–14.
- Rowley, D. B., Forte, A. M., Moucha, R., Mitrovica, J. X., Simmons, N. A., & Grand, S. P. (2013). Dynamic topography change of the eastern United States since 3 million years ago. *Science*, 340(6140), 1560–1563. <https://doi.org/10.1126/science.1229180>
- Roy, M., Jordan, T. H., & Pederson, J. L. (2009). Colorado Plateau magmatism and uplift by warming of heterogeneous lithosphere. *Nature*, 459(7249), 978–82. <https://doi.org/10.1038/nature08052>
- Royden, L., & Perron, J. T. (2013). Solutions of the stream power equation and application to the evolution of river longitudinal profiles. *Journal of Geophysical Research: Earth Surface*, 118, 497–518. <https://doi.org/10.1002/jgrf.20031>
- Rudge, J. F., Roberts, G. G., White, N. J., & Richardson, C. N. (2015). Uplift histories of Africa and Australia from linear inverse modeling of drainage inventories. *Journal of Geophysical Research: Earth Surface*, 120, 894–914. <https://doi.org/10.1002/2014JF003297>
- Sahagian, D. (1987). Epeirogeny and eustatic sea level changes as inferred from Cretaceous shoreline deposits: Applications to the central and western United States. *Journal of Geophysical Research*, 92, 4895–4904. <https://doi.org/10.1029/JB092iB06p04895>
- Salles, T. (2015). Badlands: A parallel basin and landscape dynamics model. *SoftwareX*, 5, 195–202. <https://doi.org/10.1016/j.softx.2016.08.005>
- Salles, T., Flament, N., & Muller, D. (2017). Influence of mantle flow on the drainage of eastern Australia since the Jurassic Period. *Geochemistry, Geophysics, Geosystems*, 18, 280–305. <https://doi.org/10.1002/2016GC006617>
- Schaeffer, A. J., & Lebedev, S. (2013). Global shear speed structure of the upper mantle and transition zone. *Geophysical Journal International*, 149, 417–449.
- Schildgen, T. F., van der Beek, P. A., Sinclair, H. D., & Thiede, R. C. (2018). Spatial correlation bias in late-Cenozoic erosion histories derived from thermochronology. *Nature*, 559(7712), 89–93. <https://doi.org/10.1038/s41586-018-0260-6>
- Self, R. P. (1977). Longshore variation in beach sands, Nautla Area, Veracruz, Mexico. *Journal of Sedimentary Research*, 47(4), 1437–1443. <https://doi.org/10.1306/212F7388-2B24-11D7-8648000102C1865D>
- Setterholm, D. R. (1994). The Cretaceous rocks of southwestern Minnesota: Reconstructions of a marine to nonmarine transition along the eastern margin of the Western Interior Seaway. In G. W. Shurr, G. W. Ludvigson, & R. H. Hammond (Eds.), *Perspect. East. Margin Cretaceous West. Inter. Seaw.* (Vol. 287, pp. 97–110). Boulder, CO: Geological Society of America Special Paper.
- Shen, W., & Ritzwoller, M. H. (2016). Crustal and uppermost mantle structure beneath the United States. *Journal of Geophysical Research: Solid Earth*, 121, 4306–4342. <https://doi.org/10.1002/2016JB012887>
- Sklar, L., & Dietrich, W. E. (1998). River longitudinal profiles and bedrock incision models: Stream power influence of sediment supply. *Rivers Over Rock: Fluvial Processes in Bedrock Channels (Geophysical Monograph Series)*, 107, 237–260.
- Sklar, L. S., & Dietrich, W. E. (2001). Sediment and rock strength controls on river incision into bedrock. *Geology*, 29(12), 1087–1090.
- Slone, J., Henry, C. D., Hopkins, M., & Ludington, S. Original database by Zartman, R. E., C. A. Bush and C. Abston (2003), National Geochronological Database (U.S. Geological Survey Open-file Report, 03-236). <https://pubs.usgs.gov/of/2003/0236>
- Smith, A. G., Smith, D. G., & Funnell, B. M. (1994). *Atlas of Mesozoic and Cenozoic coastlines*, pp. 99. United Kingdom: Cambridge University Press.
- Snyder, W. S., Dickinson, W. R., & Silberman, M. L. (1976). Tectonic implications of space-time patterns of Cenozoic magmatism in the Western United States. *Earth and Planetary Science Letters*, 32, 91–106.
- Snyder, N. P., Whipple, K., Tucker, G., & Merrits, D. (2000). Landscape response to tectonic forcing: DEM analysis of stream profiles in the Mendocino triple junction region, northern California. *Geological Society of America Bulletin*, 112(8), 1250–1263. [https://doi.org/10.1130/0016-7606\(2000\)112<1250:LRTTFD>2.3.CO;2](https://doi.org/10.1130/0016-7606(2000)112<1250:LRTTFD>2.3.CO;2)
- Spasojević, S., & Gurnis, M. (2012). Sea level and vertical motion of continents from dynamic Earth models since the Late Cretaceous. *American Association of Petroleum Geologists Bulletin*, 96(11), 2037–2064. <https://doi.org/10.1306/03261211121>
- Spasojević, S., Liu, L., & Gurnis, M. (2009). Adjoint models of mantle convection with seismic, plate motion, and stratigraphic constraints: North America since the Late Cretaceous. *Geochemistry, Geophysics, Geosystems*, 10, Q05W02. <https://doi.org/10.1029/2008GC002345>
- Spencer, J. E. (1996). Uplift of the Colorado Plateau due to lithosphere attenuation during Laramide low-angle subduction. *Journal of Geophysical Research*, 101(13), 13595–13609. <https://doi.org/10.1029/96JB00818>
- Stephenson, S. N., Roberts, G. G., Hoggard, M. J., & Whitaker, A. C. (2014). A Cenozoic uplift history of Mexico and its surroundings from longitudinal river profiles. *Geochemistry, Geophysics, Geosystems*, 15, 4734–4758. <https://doi.org/10.1002/2014GC005425>
- Stone, D. S. (1993). Basement-involved thrust-generated folds as seismically imaged in the subsurface of the central Rocky Mountain foreland. *Geological Society of America Special Papers*, 280, 271–318.
- Tachikawa, T., Kaku, M., Iwasaki, A., Gesch, D., Oimoen, M., Zhang, Z., et al. (2011). ASTER digital elevation model version 2—Summary of validation results.
- Tapley, B., Ries, J., Bettadpur, S., Chambers, D., Cheng, M., Condi, F., et al. (2005). GGM02—An improved Earth gravity field model from GRACE. *Journal of Geodynamics*, 79, 467–478. <https://doi.org/10.1007/s00190-005-0480-z>
- Taylor, J. P., & Fitzgerald, P. G. (2011). Low-temperature thermal history and landscape development of the eastern Adirondack Mountains, New York: Constraints from apatite fission-track thermochronology and apatite (U-Th)/He dating. *Bulletin Geological Society of America*, 123(3-4), 412–426. <https://doi.org/10.1130/B30138.1>
- Thompson, G. A., & Zoback, M. L. (1979). Regional geophysics of the Colorado Plateau. *Tectonophysics*, 61(1-3), 149–181. [https://doi.org/10.1016/0040-1951\(79\)90296-8](https://doi.org/10.1016/0040-1951(79)90296-8)
- van Wijk, J. W., Baldridge, W. S., van Hunen, J., Goes, S., Aster, R., Coblenz, D. D., et al. (2010). Small-scale convection at the edge of the Colorado Plateau: Implications for topography, magmatism, and evolution of Proterozoic lithosphere. *Geology*, 38, 611–614.
- Wakabayashi, J., & Sawyer, T. L. (2001). Stream incision, tectonics, uplift, and evolution of topography of the Sierra Nevada, California. *Journal of Geology*, 109(5), 539–562.
- Weissel, J. K., & Seidl, M. A. (1998). Inland propagation of erosional escarpments and river profile evolution across the southeast Australian passive continental margin. *Geophysical Monograph - American Geophysical Union*, 107, 189–206.
- Wernicke, B. P. (1992). Cenozoic extensional tectonics of the U.S. Cordillera. In B. C. Burchfiel, P. W. Lipman, & M. L. Zoback (Eds.), *Cordilleran Orogen Conterminous U.S.* (Vol. G-3, pp. 553–581), *The Geology of North America*. Boulder, CO: Geological Society of America.

- Whipple, K. X., & Tucker, G. E. (1999). Dynamics of the stream-power river incision model: Implications for height limits of mountain ranges, landscape response timescales, and research needs. *Journal of Geophysical Research*, 104(B8), 17,661–17,674. <https://doi.org/10.1029/1999JB900120>
- Whittaker, A. C., & Boulton, S. J. (2012). Tectonic and climatic controls on knickpoint retreat rates and landscape response times. *Journal of Geophysical Research*, 117, F02024. <https://doi.org/10.1029/2011jf002157>
- Wickert, A. D. (2016). Reconstruction of North American drainage basins and river discharge since the Last Glacial Maximum. *Earth Surface Dynamics*, 4(4), 831–869. <https://doi.org/10.5194/esurf-4-831-2016>
- Willett, S. D., McCoy, S. W., & Beeson, H. W. (2018). Transience of the North American High Plains landscape and its impact on surface water. *Nature*, 561, 528–532. <https://doi.org/10.1038/s41586-018-0532-1>
- Willett, S. D., McCoy, S. W., Perron, J. T., Goren, L., & Chen, C. Y. (2014). Dynamic reorganization of river basins. *Science*, 345(6175), 1248,765–1248,765. <https://doi.org/10.1126/science.1248765>
- Wilson, D., Aster, R., Ni, J., Grand, S., West, M., Gao, W., et al. (2005). Imaging the seismic structure of the crust and upper mantle beneath the Great Plains, Rio Grande Rift, and Colorado Plateau using receiver functions. *Journal of Geophysical Research*, 110, B05306. <https://doi.org/10.1029/2004JB003492>
- Winn, C., Karlstrom, K. E., Shuster, D. L., Kelley, S., & Fox, M. (2017). 6 Ma age of carving Westernmost Grand Canyon: Reconciling geologic data with combined AFT, (U-Th)/He and  $^{40}\text{He}/^{3}\text{He}$  thermochronologic data. *Earth and Planetary Science Letters*, 474, 257–271. <https://doi.org/10.1016/j.epsl.2017.06.051>
- Wobus, C. W., Whipple, K. X., Kirby, E., Snyder, N., Johnson, J., Spyropoulos, K., et al. (2006). Tectonics from topography: Procedures, promise, pitfalls. In S. D. Willett, N. Hovius, N. T. Brandon, & D. M. Fisher (Eds.), *Tectonics, climate, and landscape evolution: Geological Society of America Special Paper* 398 (pp. 55–74), Penrose Conference Series. America: Yale Campus Press. [https://doi.org/10.1130/2006.2398\(04\)](https://doi.org/10.1130/2006.2398(04))
- Wolfe, J. A., Forest, C. E., & Molnar, P. (1998). Paleobotanical evidence of Eocene and Oligocene paleoaltitudes in midlatitude western North America. *Bulletin Geological Society of America*, 110(5), 664–678. [https://doi.org/10.1130/0016-7606\(1998\)110<0664:PEOEAO>2.3.CO;2](https://doi.org/10.1130/0016-7606(1998)110<0664:PEOEAO>2.3.CO;2)
- Ziegler, A., Rowley, D., Lottes, A., Sahagian, D., Hulver, M., & Gierlowski, T. (1985). Paleogeographic interpretation: With an example from the mid-Cretaceous. *Annual Review of Earth and Planetary Sciences*, 13, 385–425. <https://doi.org/10.1146/annurev.earth.13.1.385>
- Zoback, M. L., Thompson, G. A., & Anderson, R. E. (1981). Cainozoic evolution of the state of stress and style of tectonism of the Basin and Range province of the western United States. *Philosophical Transactions of the Royal Society A, Mathematical Physical Science*, 300(1454), 407–434.